DCC# T0900486-v5 **February 15, 2011**

LASER INTERFEROMETER GRAVITATIONAL WAVE OBSERVATORY

LIGO Laboratory / LIGO Scientific Collaboration

IO Stray Light Analysis and Baffle Design

R. Martin, L. Williams, J. Gleason, P. Sainathan, M. Arain,
D. Feldbaum, G. Ciani, M. Heintze, G. Mueller, D. Reitze, D. Tanner

University of Florida, Gainesville, FL 32611

Distribution of this document: LIGO Internal Collaboration
This is an internal working note of the LIGO Laboratory

California Institute of Technology
LIGO Project - MS 18-34
1200 E. California Blvd.
Pasadena, CA 91125
Phone (626) 395-2129
Fax (626) 304-9834
E-mail: info@ligo.caltech.edu

Massachusetts Institute of Technology
LIGO Project - NW22-295
185 Albany St.
Cambridge, MA 02139
Phone (617) 253-4824
Fax (617) 253-7014
E-mail: info@ligo.mit.edu

LIGO Hanford Observatory
P.O. Box 1970
Mail Stop S9-02
Richland, WA 99352
Phone (509) 372-8106
Fax (509) 372-8137

LIGO Livingston Observatory
P.O. Box 940
Livingston, LA 70754
Phone (225) 686-3100
Fax (225) 686-7189

http://www.ligo.caltech.edu/

Contents

I. INTRODUCTION

A. Purpose

The purpose of this document is to present a baffle design for the IO section that provides beam parking, assures component protection from high power beams, and meets the scattering requirements per LIGO-T0900501.

This baffle design presented in this document is specific to the straight interferometers L1 and H1. The conceptual design for the baffles and beam dumps for H2 will be similar, except for their location, which will be determined when the layout for the folded interferometer is final.

We have performed a thorough analysis of different scenarios when combinations of suspended optics swing simultaneously. There are a very large number of possible mirror orientations in the IO, and while we feel that our analysis is thorough, it might not be exhaustive. This affects both scattering and damage by high power beams; the latter is of particular concern. During the IO commissioning, we will experimentally verify that the beams paths are well tracked and safely blocked, before proceeding with high power operations.

B. Scope

The ray trace analysis was performed in ZEMAX [1], based on the SolidWorks layout and coordinates for the IO and COC optics [2], and optics parameters in accordance with their specifications ([3], [4]). Some parameters might have changed over the course of the analysis (like ITM wedge angle, some solid angles, and beam heights) but conceptually, they do not affect the baffle design.

IO is responsible for the baffle design in the HAM2, HAM3, and HAM8, HAM9 chambers.

IO is not responsible for the large COC baffling, and the signal recycling cavity baffles. Also, the mode cleaner tube baffle between HAM2-HAM3 chambers and HAM8-HAM9 chambers is the responsibility of AOS.

C. Wedge Angles Used for ZEMAX Modeling

TABLE I: Wedge Angles

Optic	Wedge Angle (deg)	Orientation	Direction	Symmetry
MC1	0.5	horizontal	thick side -y*	HR face perp. to cylinder axis
MC2	0.5	horizontal	thick side +y	HR face perp. to cylinder axis
MC3	0.5	horizontal	thick side +y*	HR face perp. to cylinder axis
SM1	0.5	horizontal	thick side r.h.s arrow**	HR face perp. to cylinder axis
PMMT1	0.5	horizontal	thick side r.h.s arrow**	HR face perp. to cylinder axis
PMMT2	0.5	horizontal	thick side r.h.s arrow**	HR face perp. to cylinder axis
SM2	0.5	horizontal	thick side r.h.s arrow**	HR face perp. to cylinder axis
PRM	1.0	vertical	thick side down	HR face perp. to cylinder axis
PR2	1.0	vertical	thick side down	HR face perp. to cylinder axis
BS	0.065	horizontal	thick side (+x,+y)	BS face perp. to cylinder axis
CPX	0.04	horizontal	thick side -y	AR-ITMX face perp. to cylinder axis
ITMX	0.08	vertical	thick side down	HR face perp. to cylinder axis
CPY	0.04	horizontal	thick side -x	AR-ITMY face perp. to cylinder axis
ITMY	0.08	vertical	thick side down	HR face perp. to cylinder axis
				*thin sides toward each other
				**arrow on top

D. Range of Motion for Suspended Optics

Table II shows the Range Of Motion for different suspended optics, determined by 1 mm separation of the earthquake stops, with the exception of the HSTS optics, for which we used 0.635 mm separation.

TABLE II: Suspended Optics Range of Motion

Suspension	Vertical ROM (mrad)	Vertical ROM (deg)	Horizontal ROM (mrad)	Horizontal ROM (deg)
Quad (ITM)	+/-6.89	+/-0.395	+/-6.89	+/-0.395
HAM Aux (SM, PMMT)	+/-31.24	+/-1.790	+/-75.41	+/-4.321
HSTS (MC, RM)	+/-11.87	+/-0.68	+/-21.47	+/-1.23
HLTS (PR3)	+/-10.27	+/-0.59	+/-13.94	+/-0.80

In addition, the 6" mirror control range (which determines the parking position of the beam when PRC not locked by misaligning the PRM) is determined by the OSEMS range [5] shown in Table III.

TABLE III: PRM Control Range

Yaw (mrad)	Pitch (mrad)	Yaw (deg)	Pitch (deg)
4.10	2.55	0.235	0.146

E. General Acronyms

AOI	Angle Of Incidence
AOS	Auxiliary Optics Support
AOSc	Angle Of Scatter
BRDF	Bidirectional Reflectance Distribution Function
BS	Beam splitter
DKDP	Deuterium Potasium Di-Hydrogen Phosphate
FI	Faraday Isolator
FR	Faraday Rotator
HAM	Horizontal Access Module
HAM Aux	Auxiliary Suspensions
IO	Input Optics
ISS-PDs	Intensity Stabilization Photodiodes
ITM	Input Test Mass
OSEM	Optical Sensor Electromagnetic Motor
PRC	Power Recycling Cavity
PSS	Porcelain-coated (Stainless) Steel
ROM	Range of Motion
SiC	Silicon Carbide
SP	Septum Plate
TGG	Terbium Gallium Garnet
VP	View Port

F. Baffle Labels

Beam Dumps	
V1	Parking Beam Dump
V2	Beam Dump for the Depolarization in the Faraday Isolator
V3	REFL Beam Dump
Suspension Baffles	
BW1	SM1 Front Baffle
BW2	PMMT1 Front Baffle
BW3	PMMT2 Front Baffle
BW4	SM2 Front Baffle
BW5	SM2 Front Baffle Insert
BW11	PRM-AR Baffle
–	HAM2 and HAM3 Table Baffle
Hard Apertures and Protective Plates	
HA1	HWP1 from SM1
HA2-a	AOE1 from SM1
HA2-b	AOE1 from PMMT1
HA3	FI-In
HA4	FR-In
HA5	FR-Out
HA6	FI-Out
HA7-Top/Bottom	MC REFL Periscope 1 baffles
HA8-Top/Bottom	MC REFL Periscope 2 baffles
HA9	between PMMT2 and SM2
HA11	ISS-PD baffle
HA12-a	AOE2-In
HA12-b	AOE2-Out
HA13	IO REFL walk-off
P1	PMMT1 swings toward SM1
P2	PMMT2 swings toward IO Periscope
Scrapper Baffles	
MC-Z	Scraper Baffle for the Input Mode Cleaner Cavity
PRC-Z	Scraper Baffle for the Power Recycling Cavity

Ghost Beam Baffles

GBB1	SP-VP Window AR-specular
GBB2	S1 HR-transmitted
GBB3	S2 HR-transmitted
GBB4	MC1-AR specular
GBB5	MC3-AR Faraday Isolation
GBB6	SM1-HR trans return
GBB7	PMMT1 HR-transmitted
GBB8	PMMT2 HR-transmitted
GBB9	MC2 HR-trans, M-HR transmitted
GBB10	MC2 HR-trans VP-AR specular
GBB11	PR2 HR-trans M1-transmitted
GBB12	PR2 HR-trans M2-transmitted
GBB13	PR2 HR-trans M3-transmitted

II. IO IN-VACUUM BAFFLES

The IO baffles in Advanced LIGO will have several purposes: to safely park high and/or low power beams, to protect optical components and equipment from being hit by high power beams and to reduce the amount of stray light in the interferometer when this is in Science mode.

Based on their purpose, we design the following types of baffles:

1. **Beam Dumps**, for parking and dumping high power beams, and storing lower power beams during the interferometer operation;

2. **Suspension Baffles**, for protecting suspension wires and equipment when high power beams move as suspended optics swing.

3. **Hard Apertures and Plates**, for farther preventing the high power beams from hitting sensitive optics and equipment.

4. **Scraper Baffles**, for collecting the light scattered under small angle and preventing it from resonating off-axis inside the mode cleaner and the power recycling cavity.

5. **Ghost Beam Baffles**, for blocking specular reflections from AR coatings and other low power beams.

III. OPTICAL LAYOUT OF THE HAM2 AND HAM3 TABLES

The most up-to-date SolidWorks layouts for the HAM2 and HAM3 tables are shown in Figures 1 and 2.

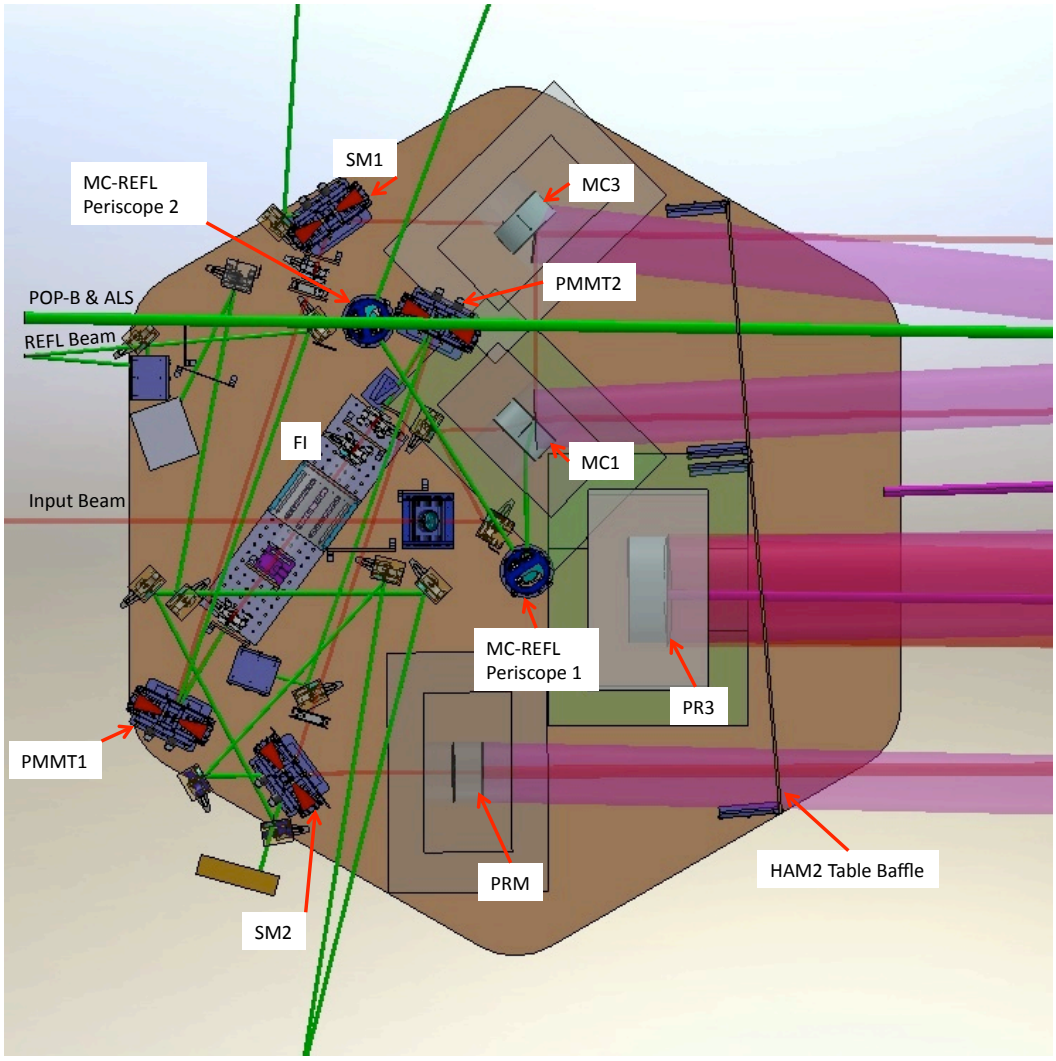

FIG. 1: SolidWorks layout of the Advanced LIGO HAM2 table

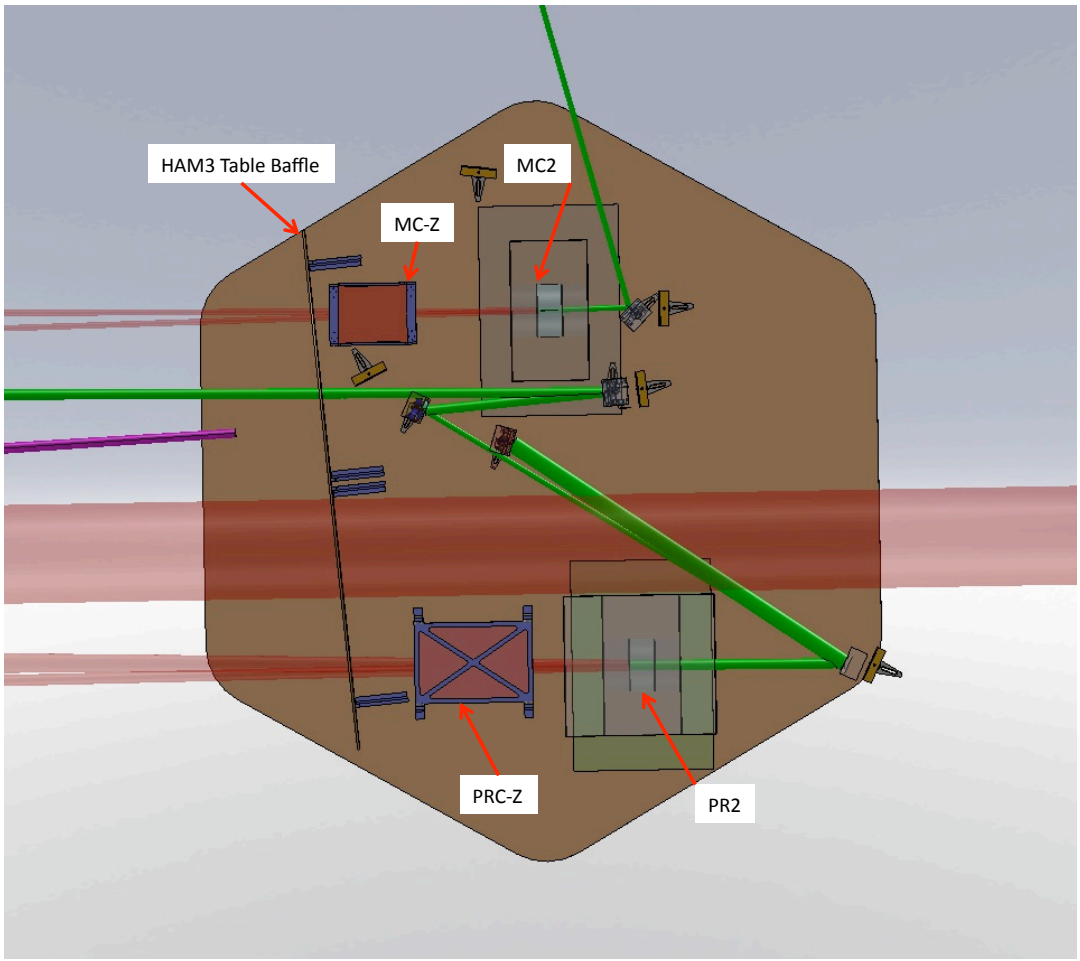

FIG. 2: SolidWorks layout of the Advanced LIGO HAM3 table

IV. BAFFLE DESIGNS AND PERFORMANCE

A. Beam Dumps

There are three in-vacuum beam dumps in IO section: parking beam dump, beam dump for storing the residual depolarization in the Faraday isolator, and the REFL beam dump. These are discussed in detail in the following sections.

1. *Parking Beam Dump (V1)*

The parking beam dump stores the high power beam reflected by PRM when the interferometer is purposely misaligned, while the mode cleaner is still locked. In this case, the scattering produced by it is not an immediate concern, but should still be minimized so that it does not interfere with the alignment and sensing controls while testing or re-locking the interferometer or with the PSL intensity stabilization servo sensing photodiode (ISS PD). **NOTE: Based on an FEA estimate of the temperature rise of the beam dump and HAM ISI platform, we are most likely going to route the parking beam to outside the vacuum and dump it on IOT2B. Once the design change is confirmed, we will update this document.**

Operating Conditions: Interferometer is not locked. When the beam is parked, V1 is normally illuminated with up to 150 W.

Location: The parking beam dump is placed between the hard aperture HA6 of the Faraday isolator and PMMT2, as shown in Figure 3.

It is designed in a V shape, oriented with the vertex in the vertical plane, as shown in Figure 4.

The main parameters for this beam dump are summarized in Table IV.

TABLE IV: Parking Beam Dump Parameters

Optical Power	150 W
Beam size at the baffle	w_h = 5.18 mm, w_v = 1.95 mm
Mximum Optical Intensity	475 W/cm^2
Polarization	p (Horizontal w.r.t the plane of IFO)
	Electric field in the baffle plane of incidence
PRM Control Range (from center)	Yaw: ± 4.10 mrad (±0.235 deg)
	Pitch: ± 2.55 mrad (±0.146 deg)
Drawing DCC #	D0902375
ZEMAX notation on the layout (Fig. 3)	V1
Material	super-polished SiC
Refractive Index @ 1064 nm	2.575
Brewsters Angle	68.78 deg

The high power p-polarized beam hits the first surface at Brewsters angle, where 99.9% is absorbed. The reflectivity of super-polished SiC at Brewsters angle for p-polarized light was measured to be less than 0.1% (The results of the measurements are shown in Section VI Figure 20). The length of the beam dump was designed to allow for 7 bounces before the beam exits

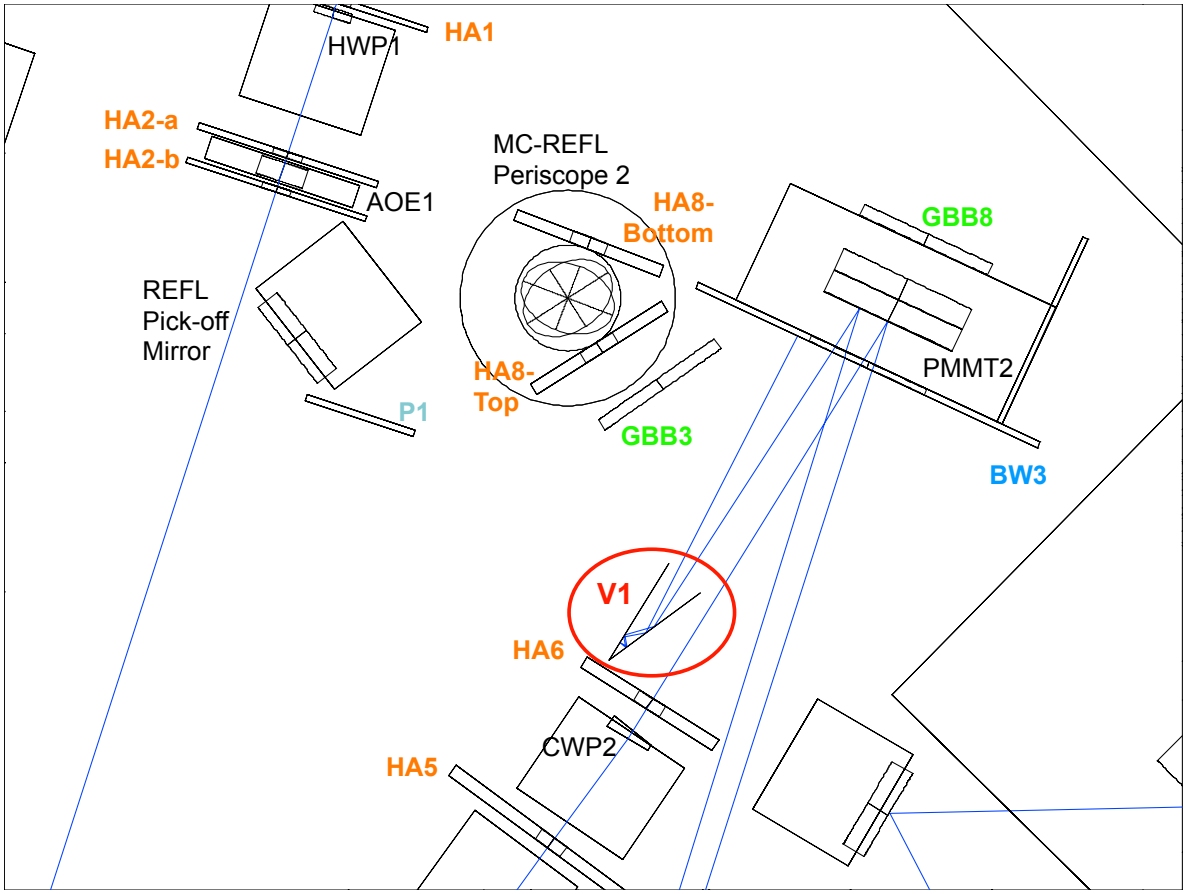

FIG. 3: Parking beam dump V1 for the beam reflected back from PRM when the interferometer looses lock and MC still locked.

carrying a fraction of about 10^{-12} of its initial power.

The beam reflected back from PRM is parked at 1 ppm clipping level, when the pitch-yaw settings of the PRM are 85% of the full extent from the center. This is 11.5 mm left and 7.2 mm below the main beam, when facing PMMT2 from the parking beam dump. The full extent is 16.2 mm left and 10.2 mm down of the main beam on HA6, for 0.235 deg yaw and 0.146 deg pitch. If more range is desired for parking, this can be accomplished with small SM2 tilt - 0.05 deg yaw would produce additional 7 mm horizontal displacement. The control range of SM2 is 10 mrad (0.573 deg).

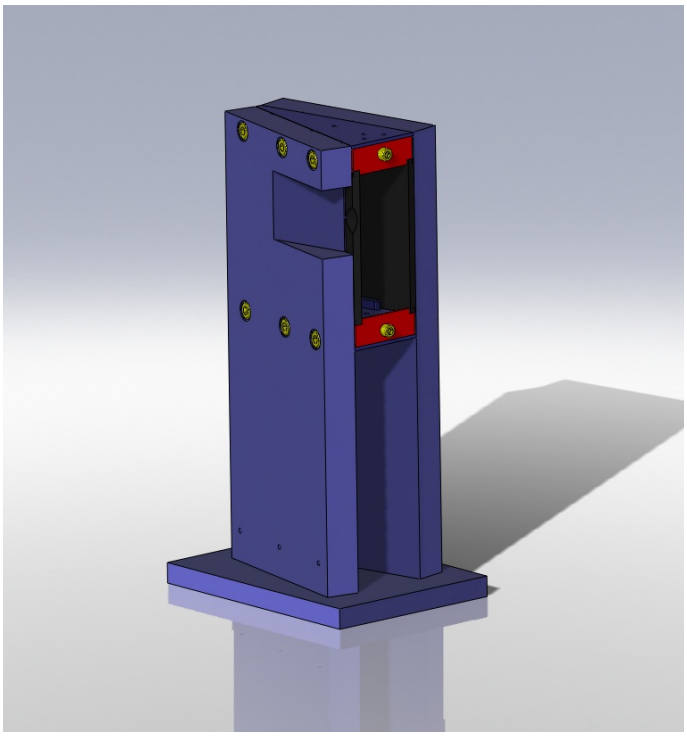

FIG. 4: Parking Beam Dump

2. Beam Dump for the Depolarization in the Faraday Isolator (V2)

It dumps the s-polarized beam produced by various polarization losses in the Faraday isolator. This beam exits the isolator at a 1.4 deg angle from the main beam.

Operating Conditions: Interferometer is locked. The expected power on this beam dump is less than 1.5 W for a maximum power of 150 W from the IMC.

Location: Between PMMT2 and SM2, as shown in Figure 5.

It is a V-shape similar to the parking beam baffle, but rotated by 90 deg w.r.t. the horizontal axis, so that its vertex is in the horizontal plane. This way the electric field of the s-polarized beam from FI is in the plane of incidence of the first surface and hits at Brewsters angle for maximized absorption. The beam will again bounce 7 times inside the baffle before it exits with roughly 10^{-12} of the incident power.

Because this beam will be resting on the V2 beam dump continuously, including when the IFO is in science mode, the scattering issue will be addressed. An analysis of the light scattering in the IO components is presented in Section V of this document.

Although the beam stored on this beam dump has very low power, the material should be

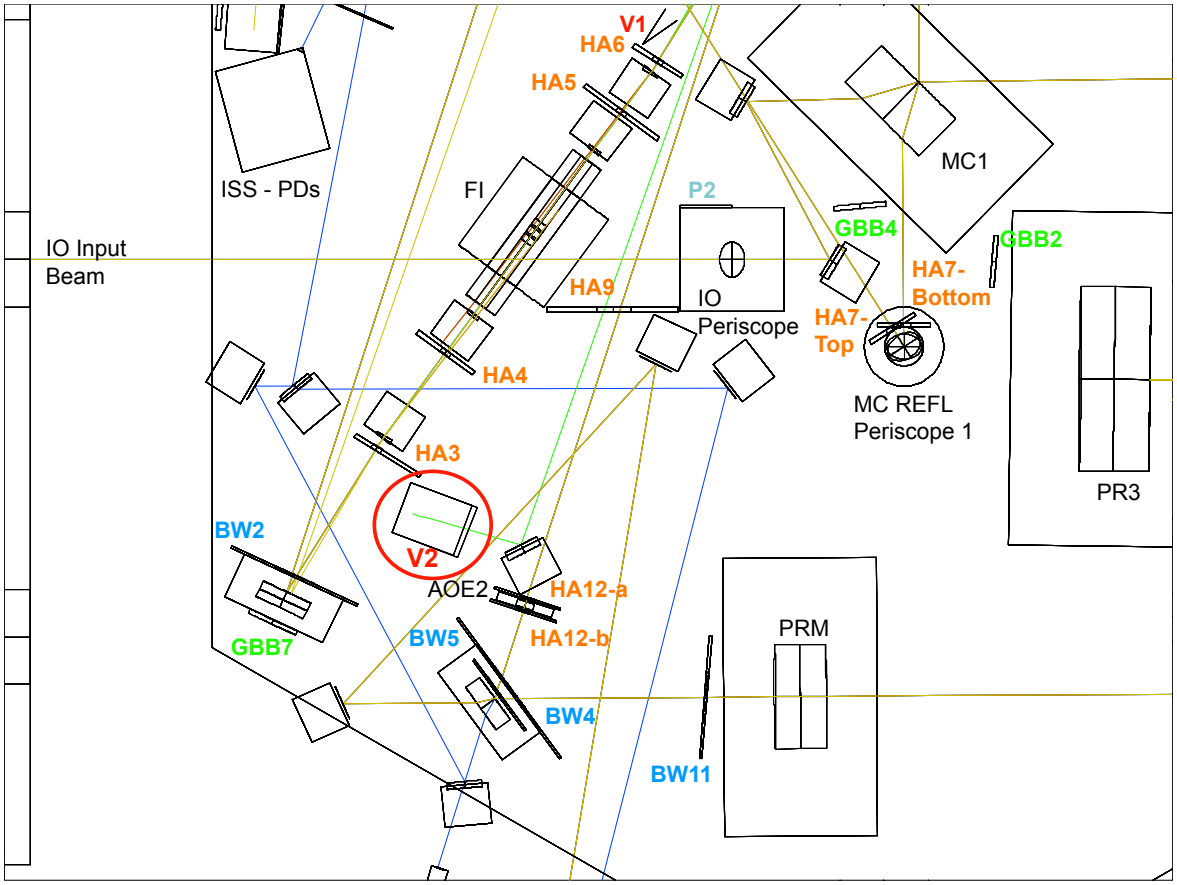

FIG. 5: The beam dump V2 for the depolarization in the Faraday isolator and other surrounding baffles

able to handle optical powers as high as 150 W when PMMT2 accidentally swings and sweeps the forward beam across its surface. Thus, this baffle needs to be make of SiC.

3. REFL Beam Dump (V3)

The REFL beam dump stores the high power beam reflected from the interferometer after it passes back through the Faraday isolator. This beam dump should handle the power when the IFO is in Science mode, as well as unlocked. **NOTE: Based on an FEA estimate of the temperature rise of the beam dump and HAM ISI platform, we are most likely going to route the REFL beam to outside the vacuum and dump it on IOT2B. Once the design change is confirmed, we will update this document.**

Operating Conditions: Interferometer is locked and unlocked. This beam dump will see as much

TABLE V: FI Losses Beam Dump Parameters

Optical Power	<1.50 W
Beam size at the baffle	w_h= 2.13 mm, w_v=5.69 mm
Polarization	s (Vertical w.r.t the plane of IFO)
	Electric field in the baffle plane of incidence
Drawing DCC #	D0902377
ZEMAX notation on the layout (Fig. 5)	V2
Material	super-polished SiC

as 4.5 W during science mode operation and up to 150 W when the interferometer is unlocked.

Location: Between REFL pick-off mirror and septum plate view port (Figure 6).

Uses the same design as the Faraday loss beam dump - V-shape with the vertex in horizontal plane as shown in Figure 7.

The parameters for this beam dump are listed in Table VI below.

TABLE VI: REFL Beam Dump Parameters

Optical Power	4.50 W (IFO locked) to 150 W (IFO unlocked)
Beam size at the baffle	w_h=2.12 mm, w_v=5.66 mm
Polarization	s (Vertical w.r.t the plane of IFO)
	Electric field in the baffle plane of incidence
Drawing DCC #	D1002585
ZEMAX notation on the layout (Fig. 6)	V3
Material	super-polished SiC

Scattering from the REFL beam dump is an issue that will be investigated (Section V), since a high power beam will be resting continuously on it, including when the interferometer is locked.

B. Suspension Baffles

These baffles block the high power beams from accidentally hitting the suspension wires, dumpers, photodiodes or other equipment of the HAM Aux and HSTS suspensions when other suspended optics swing against the earthquake stops.

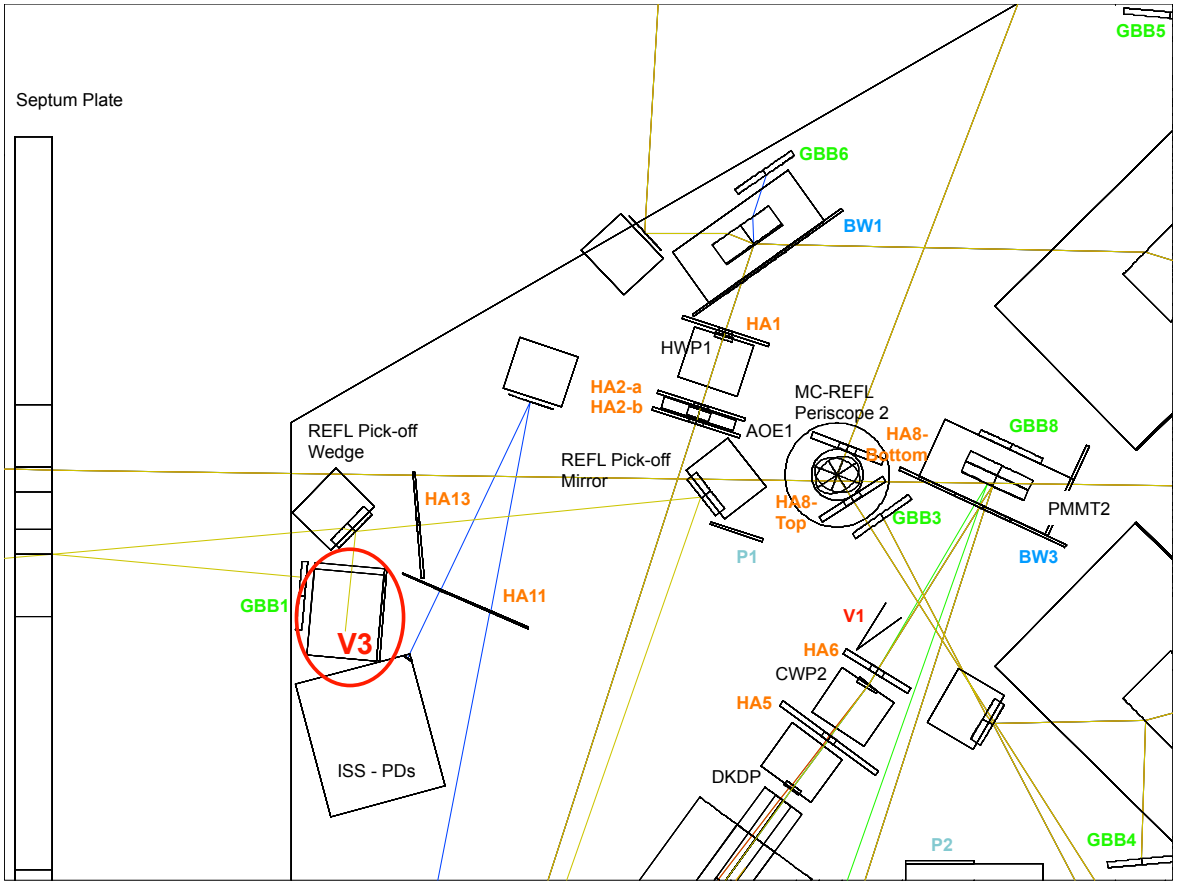

FIG. 6: REFL beam dump V3 and other surrounding baffles in HAM2

1. *SM1 Front Baffle (BW1)*

Operating Conditions: Protection baffle only; ordinarily there is no light on this baffle.

Location: Attached to the HAM Aux suspension tower.

2. *PMMT1 Front Baffle (BW2)*

Operating Conditions: Protection baffle only; ordinarily there is no light on this baffle.

Location: Attached to the HAM Aux suspension tower.

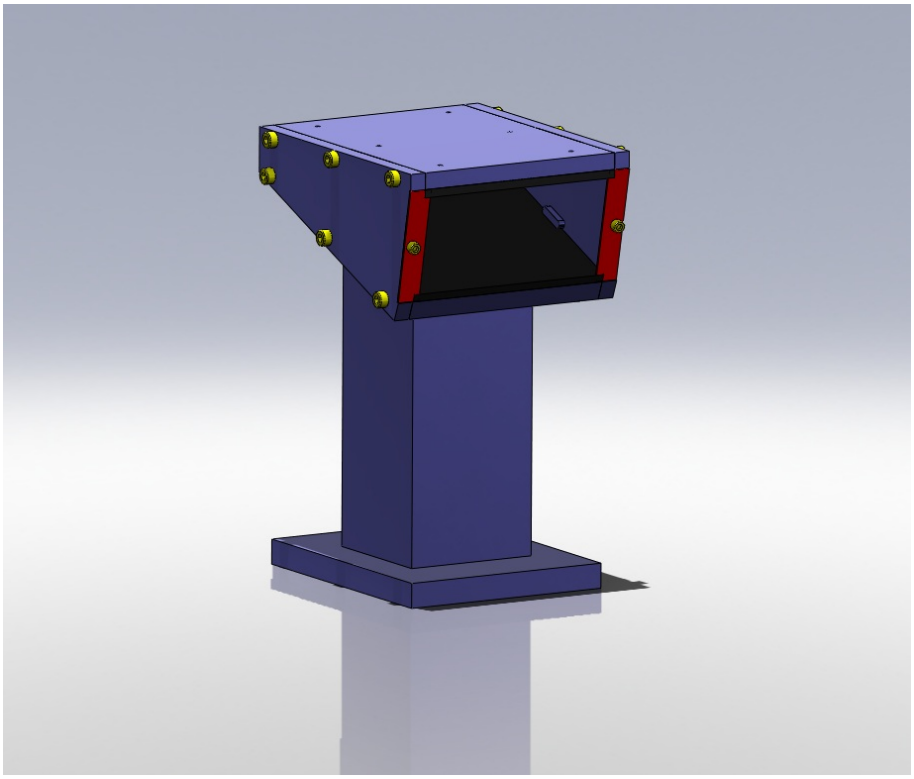

FIG. 7: REFL Beam Dump

TABLE VII: SM1 Front Baffle Parameters

Optical Power	150 W
Beam size at the baffle	$w_h = 3.54$ mm, $w_v = 2.11$ mm
Angle of Incidence	53.38 deg
Beams separation at baffle (incident-reflected)	64.46 mm
Polarization	s
Clear Aperture	110.3 mm
Drawing DCC #	D0902378
ZEMAX notation on the layout (Fig. 6)	BW1
Material	SiC, unpolished

3. PMMT2 Front Baffle (BW3)

Operating Conditions: Protection baffle only; ordinarily there is no light on this baffle.

Location: Attached to the HAM Aux suspension tower.

TABLE VIII: PMMT1 Front Baffle Parameters

Optical Power	150 W
Beam size at the baffle	w_h = 2.18 mm , w_v = 2.16 mm
Angle of Incidence	7 deg
Beams separation at baffle (incident-reflected)	5.89 mm
Polarization	p
Clear Aperture	60 mm
Drawing DCC #	D0902380
ZEMAX notation on the layout (Fig. 5)	BW2
Material	SiC, unpolished

TABLE IX: PMMT2 Front Baffle Parameters

Optical Power	150 W
Beam size at the baffle	w_h = 1.91 mm, w_v = 1.89 mm
Angle of Incidence	7 deg
Beams separation at baffle (incident-reflected)	5.95 mm
Polarization	p
Clear Aperture	67.5 mm
Drawing DCC #	D0902382
ZEMAX notation on the layout (Fig. 3, 6)	BW3
Material	SiC, unpolished

4. SM2 Front Baffle (BW4)

Operating Conditions: Protection baffle only; ordinarily there is no light on this baffle.

Location: Attached to the HAM Aux suspension tower.

TABLE X: SM2 Front Baffle Parameters

Optical Power	150 W
Beam size at the baffle	w_h = 2.63 mm, w_v = 2.13 mm
Angle of Incidence	35.89 deg
Beams separation at baffle (incident-reflected)	34.67 mm
Polarization	p
Clear Aperture	79.6 mm
Drawing DCC #	D0902745
ZEMAX notation on the layout (Fig. 5)	BW4
Material	SiC, unpolished

5. *SM2 Front Baffle Insert (BW5)*

Operating Conditions: Protection baffle only; ordinarily there is no light on this baffle.
Location: Attached to the HAM Aux suspension tower.

TABLE XI: SM2 Front Baffle Insert Parameters

Optical Power	150 W
Beam size at the baffle	$w_h = 2.63$ mm, $w_v = 2.13$ mm
Angle of Incidence	35.89 deg
Beams separation at baffle (incident-reflected)	9.19 mm
Polarization	p
Clear Aperture	58.5 mm
Drawing DCC #	D0902722
ZEMAX notation on the layout (Fig. 5)	BW5
Material	SiC, unpolished

6. *PRM-AR Baffle (BW11)*

Operating Conditions: Protection baffle only; ordinarily there is no light on this baffle.
Location: About 25 mm in front of the HAM Aux suspension tower, toward SM2.

TABLE XII: PRM-AR Baffle Parameters

Optical Power	150 W
Beam size at the baffle	w = 2.2 mm
Angle of Incidence	5 deg
Polarization	p
Clear Aperture	76.2 mm
Drawing DCC #	D1003050
ZEMAX notation on the layout (Fig. 5)	BW11
Material	SiC, unpolished

7. *HAM2 and HAM3 Table Baffles*

The HAM2 Table Baffle protects components on the HAM2 optical table from the beam's large motion across it, when MC2 or PR2 optics in the HAM 3 table swing. Similarly, the HAM3 Table

Baffle protects components in HAM3 when MC3, MC1, SM2 or combination of PRC optics or ITMs swing.

Operating Conditions: Protection baffles only; ordinarily there is no light on these baffles.

Location: At the edge of the HAM2 and HAM3 tables.

The main parameters for the HAM2 and HAM3 Table Baffles are listed in Table XIII.

TABLE XIII: HAM 2 and HAM3 Table Baffles Parameters

Optical Power	as high as 28 kW
Beam size at the baffle	w_{HAM2} = 2.1 mm - 2.2 mm (HAM2)
	w_{HAM3} = 3.38 mm - 6.2 mm (HAM3)
	w_{toIFO} = 53 mm - 54 mm
	$w_{ALS\$POP-B}$ = 2.5 mm - 3 mm
Angle of Incidence	5 deg
Polarization	p
Drawing DCC #	D1002993 (HAM2)
	D1003075 (HAM3)
Material	SiC, unpolished

C. Hard Apertures and Plates

Hard apertures and protective plates are placed systematically across the HAM2 table to block the high power beam from wondering across the table when suspended optics swing accidentally.

1. Hard apertures for the Faraday isolator and other transmissive optics (HA1-6, HA12)

Operating Conditions: Protection baffle only; ordinarily there is no light on these baffles.

Location: Various places in the IO beam path.

These hard apertures define a narrow beam propagation tube, to prevent the high power beam from hitting the indium layer that wraps around the TGG crystals, or the heaters of the adaptive optical element. In addition, these apertures help reducing the amount of stray light from propagating into the interferometer by blocking ghost beams created by these transmissive optics.

The hard apertures for the Faraday isolator (labeled HA3 through HA6) are shown in Figure 8.

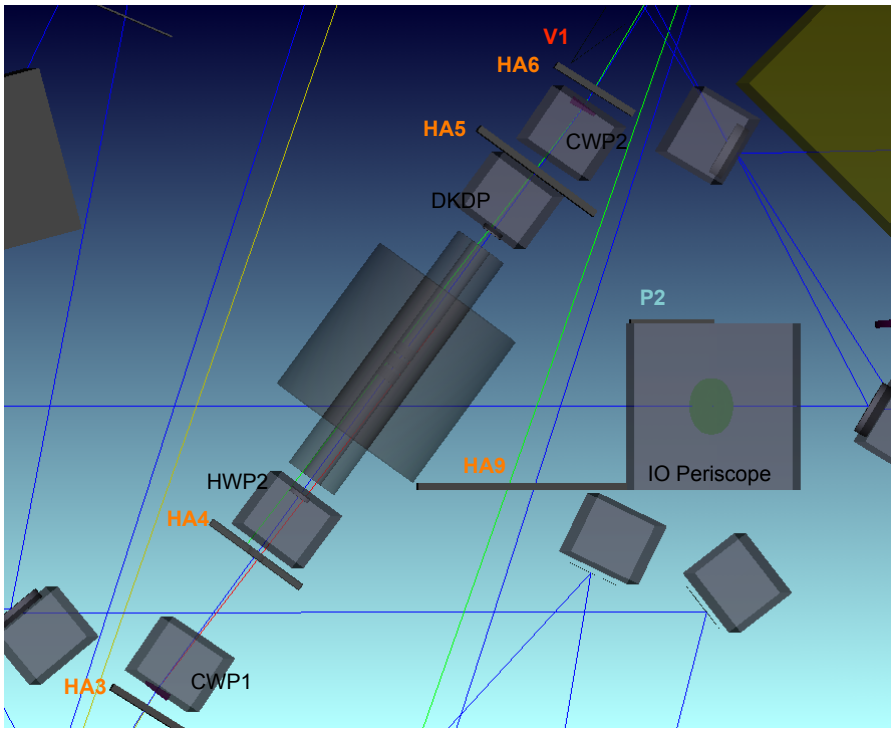

FIG. 8: Hard apertures for the Faraday isolator

A list of the hard apertures and their main parameters for FI and other small IO transmissive

optics is shown in Table XIV below.

TABLE XIV: HA1 - HA6, HA12 Parameters

Optical Power	150 W (IFO unlocked)
Beam size at the baffle	1.94 mm - 2.17 mm
Angle of Incidence	5 deg
Polarization	s and p
ZEMAX notation on the layout (Fig. 5, 3, 6)	HA1: HWP1 from SM1
	HA2-a: AOE1 from SM1
	HA2-b: AOE1 from PMMT1
	HA3: FI-In
	HA4: FR-In
	HA5: FR-Out
	HA6: FI-Out
	HA12-a: AOE2-In
	HA12-b: AOE2-Out
Clear Aperture	HA1: 15 mm
	HA2-HA6: 16 mm
	HA12-a, HA12-b: 20 mm
Drawing DCC #	HA1: D0902384
	HA2: D0902386
	HA3: D0902388
	HA4: D0902390
	HA5: D0902392
	HA6: D0902394
	HA12-a: D1002725
	HA12-b: D1002726
Material	SiC, unpolished

Hard apertures HA1 and HA2-a/b enclose the HWP1 and the AOE1, while HA3 - HA6 are placed in front and back of the Faraday isolator and after each calcite polarizer for additional limitation of the exposure angle. HA3 - HA6 determine a tube of acceptance for the high power beams inside the Faraday isolator. HA12-a/b protect the AOE2 and limit the beam walk toward PMMT2 when SM2 and PRM swing accidentally. Also they help with the PMMT2 small angle swing for the forward beam.

Our Zemax analysis shows that the low power s-pol beams from the calcite polarizers in the forward and backward directions can hit the indium layer surrounding the TGG crystals. The power in these beams is determined by the polarization mismatch between the HWP after the IMC and the first CWP of the FI for the forward beam, and between the IFO and the second CWP for the backward propagating beam.

For $P_{inc} = 150\ W$ and 2 deg mismatch between HWP1 and CWP1 or between IFO and CWP2 axis, the power carried by these beams is $P_s = 150\ W * sin^2(2deg) = 183\ mW$. This value of the optical power is completely safe for indium. Note that a 2 deg mismatch for either forward or backward beams is unrealistically large and was selected for a conservative analysis. We should not expect more than 0.5 deg mismatch (adjustment of HWP1 plus tilt of the CWP1 plane w.r.t. beam axis).

2. Hard Apertures for MC REFL - Periscope 1 and 2 Baffles (HA7-Top/Bottom, HA-8 Top/Bottom)

Operating Conditions: Protection baffle only; ordinarily there is no light on these baffles.

Location: Physically attached to the MC REFL periscopes.

These baffles prevent the high power beam incident on the input mode cleaner from swinging across the table when MC1 swings and the mode cleaner loses lock.

TABLE XV: MC REFL - Periscope 1 and 2 Baffle Parameters

Optical Power	185 W
Beam size at the baffle	2.1 mm - 2.2 mm
Angle of Incidence	5 deg
Polarization	s
Clear Aperture	20 mm
ZEMAX notation on the layout (Fig. 5, 3, 6)	HA7-Top/Bottom (Periscope 1)
	HA8-Top/Bottom (Periscope 2)
Drawing DCC #	D1002689
Material	SiC, unpolished

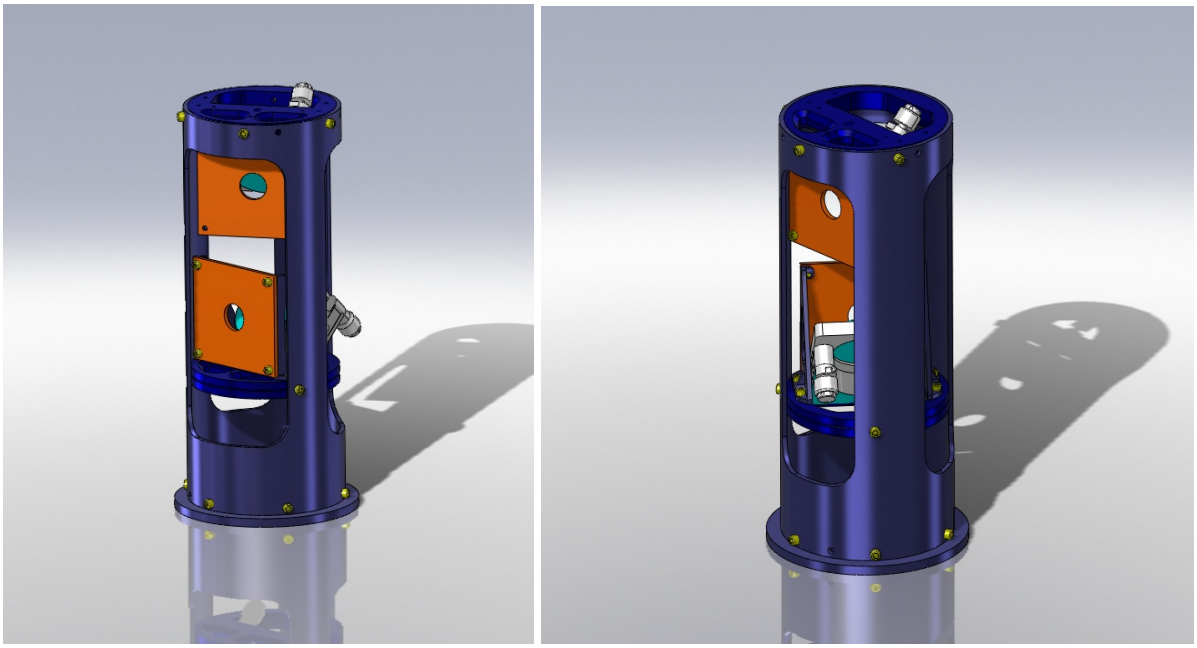

(a) (b)

FIG. 9: MC REFL Periscope Baffles - (a) HA-7 Top/Bottom for Periscope 1, and (b) HA-8 Top/Bottom for Periscope 2

3. Supplementary Hard Apertures (HA9, HA11, HA13)

Operating Conditions: Protection baffles only; ordinarily there is no light on these baffles.

Location: Various places in the IO beam path.

These are miscellaneous hard apertures used for additional high power beam confinement (HA9 for the beam between PMMT2 and SM2, HA13 for the REFL beam walk-off) or stray light control (HA13 to limit scattering into the ISS-PDs). Their parameters are listed in Table XVI below.

4. Plates (P1, P2)

Operating Conditions: Protection baffle only; ordinarily there is no light on the these baffles.

Location: Various places in the IO beam path.

Plates offer additional protection at locations that the high power beam reaches only when optics swing far from their optimum alignment. In particular, plate P1 is placed right in front of the REFL pick-off mirror to block the forward going beam reflected off PMMT1 when PMMT1 swings toward SM1. Plate P2 is attached to the IO periscope to block the same beam when PMMT2 swings toward SM2.

TABLE XVI: Supplementary Hard Apertures Parameters

Parameter	HA9 (SM2 to PMMT2)	HA11 (ISS-PD baffle)	HA13 (IO REFL walk-off)
Optical Power	150 W	< 10 mW	4.5 W - 150 W
Beam size at the baffle	2.07 mm	2.2 mm	2.12 mm
Angle of Incidence	18 deg	5 deg	5 deg
Polarization	p	p	s
Clear Aperture	d_h=50 mm, d_v=20 mm	16 mm	16 mm
Drawing DCC#:	D1002557	D1002724	D1002999
Material	SiC, unpolished	PSS	SiC, unpolished

TABLE XVII: Protective Plates Parameters

Optical Power	150 W
Beam size at the baffle	1.9 mm - 2.1 mm
Angle of Incidence	5 deg
Polarization	p
Clear Aperture	N/A
ZEMAX notation on the layout (Fig. 5, 6)	P1: PMMT1 swing toward SM1
	P2: PMMT2 swing toward IO Periscope
Drawing DCC #	P1: D1003000
	P1: D1003001
Material	SiC, unpolished

D. Scraper Baffles

Scraper baffles collect the light scattered under small angle to prevent it from resonating off axis in the mode cleaner and power recycling cavities. In addition, these scraper baffles catch ghost beams due to AR coating from PR2, ITM, CP, and BS (PRC-Z). For optimum collection of the stray light propagating close to the main beam, these baffles are designed at Brewster's angle, aligned for the polarization in that particular optical cavity.

A ZEMAX layout showing the scraper baffles and other ghost beam baffles in HAM3 is shown in Figure 10.

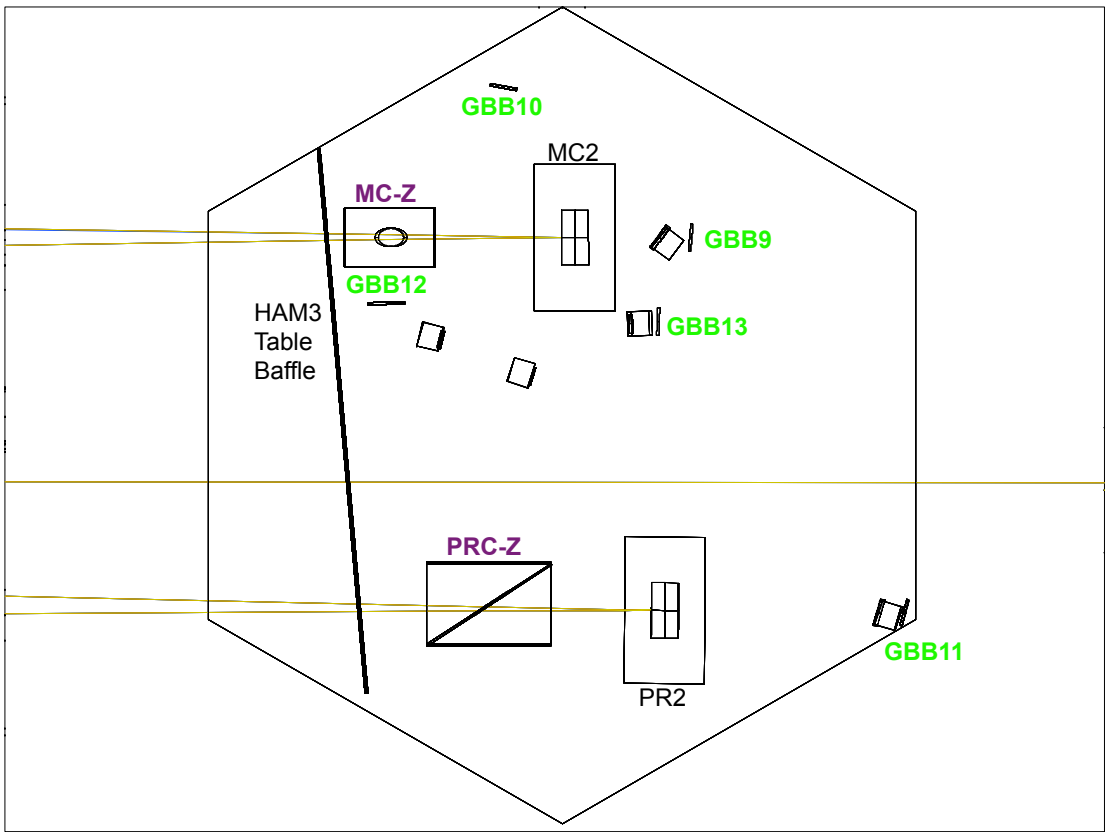

FIG. 10: HAM3 Scrapper and Ghost Beam Baffles

1. *Scraper Baffle for the Input Mode Cleaner Cavity (MC-Z)*

Operating Conditions: Mode filter baffle; will see less than 3 W when IMC is locked and properly aligned; as much as 1 W when unlocked.

Location: MC-Z is a stand alone baffle, placed at about 470 mm in front of MC2.

The MC-Z baffle design is shown in Figure 11.

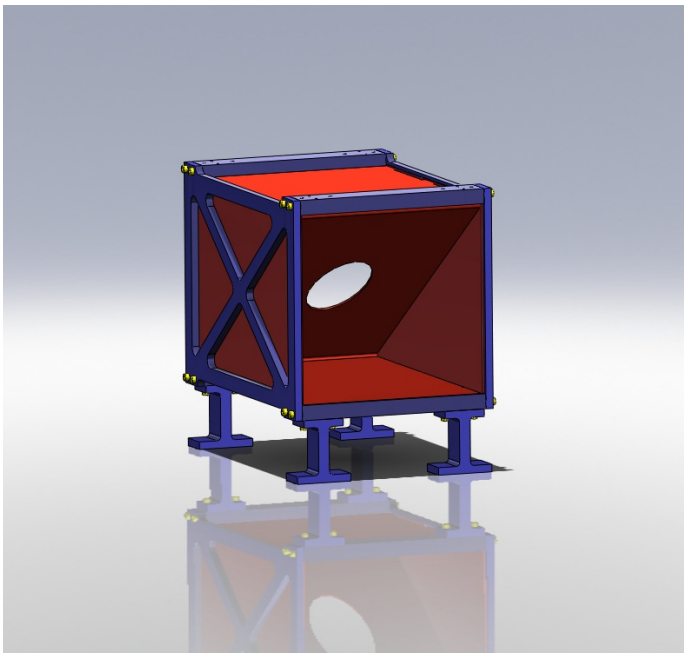

FIG. 11: Input Mode Cleaner Scraper Baffle (MC-Z)

The main parameters of the mode cleaner scraper baffle are listed in Table XVIII.

TABLE XVIII: MC-Z Baffle Parameters

Optical Power	<3 W at 100 ppm clipping - IMC locked
	1 W - IMC unlocked
Beam size at the baffle	3.38 mm
Angle of Incidence	57 deg
Beams separation at baffle	23.5 mm
Polarization	s
Clear Aperture	50 mm, in the vertical plane
Drawing DCC #	D1000327
ZEMAX notation on the layout (Fig. 10)	MC-Z
Material	PSS

2. Scraper Baffle for the Power Recycling Cavity (PRC-Z)

Operating Conditions: Mode filter baffle; will see less than 2.5 W when power recycling cavity is locked and properly aligned; as much as 4.5 W when unlocked.

Location: PRC-Z is a stand alone baffle, placed at about 450 mm in front of PR2. The PRC-Z baffle design is shown in Figure 12.

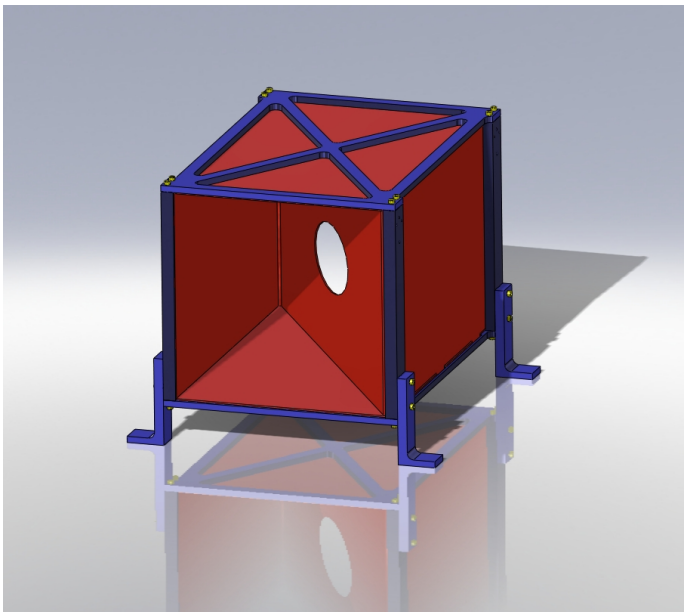

FIG. 12: Power Recycling Cavity Scraper Baffle (PRC-Z)

The main parameters of the power recycling cavity scraper baffle are listed in Table XIX.

TABLE XIX: PRC-Z Baffle Parameters

Optical Power	< 2.5 W at 500 ppm clipping - PRC locked
	4.5 W - PRC unlocked
Beam size at the baffle	6.2 mm
Angle of Incidence	57 deg
Beams separation at baffle	24.8 mm
Polarization	p
Clear Aperture	70 mm, in the vertical plane
Drawing DCC #	D1000328
ZEMAX notation on the layout (Fig. 10)	PRC-Z
Material	PSS

E. Ghost Beam Baffles (GBB1-13)

Ghost beams are caused by reflections on AR coatings and light leakage through high reflectors.

Most ghost beams in the HAM2 chamber are blocked by the SiC hard apertures and the suspension baffles BW1 – BW5 on the HAM Aux suspensions. Additional ghost beam baffles are designed to collect the remaining stray beams, when they do not end on a hard aperture, but risk to hit the walls of the chambers and eventually end on a photodiode or find ways into the IFO.

In HAM3, they are blocked by ghost beam baffles and the two scrapper baffles of the mode cleaner and the power recycling cavities.

The ghost beams with powers larger than 200 μW produced by the forward going beam (brown/green) and higher than 20 μW from the back reflected beam (blue/red) are shown in Figures 13 and 14.

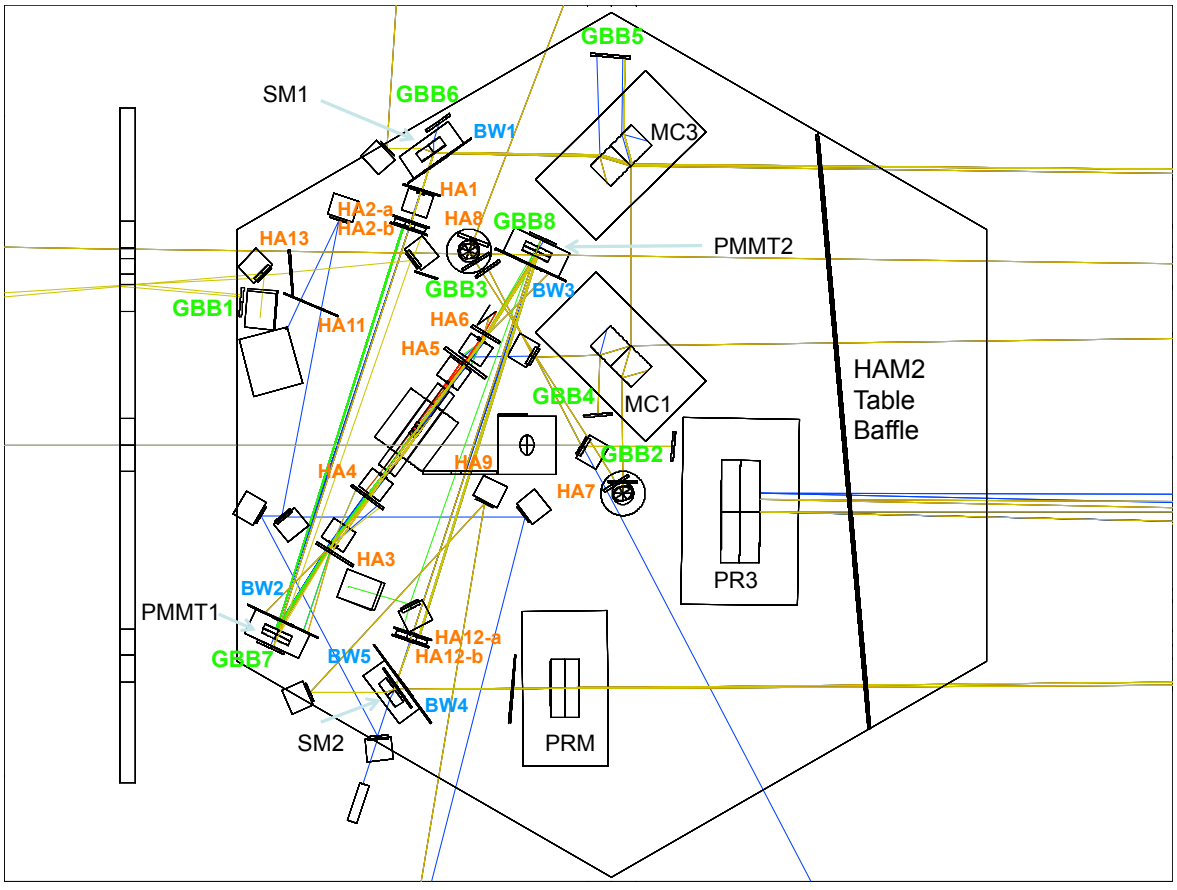

FIG. 13: Ghost beam baffles in HAM2

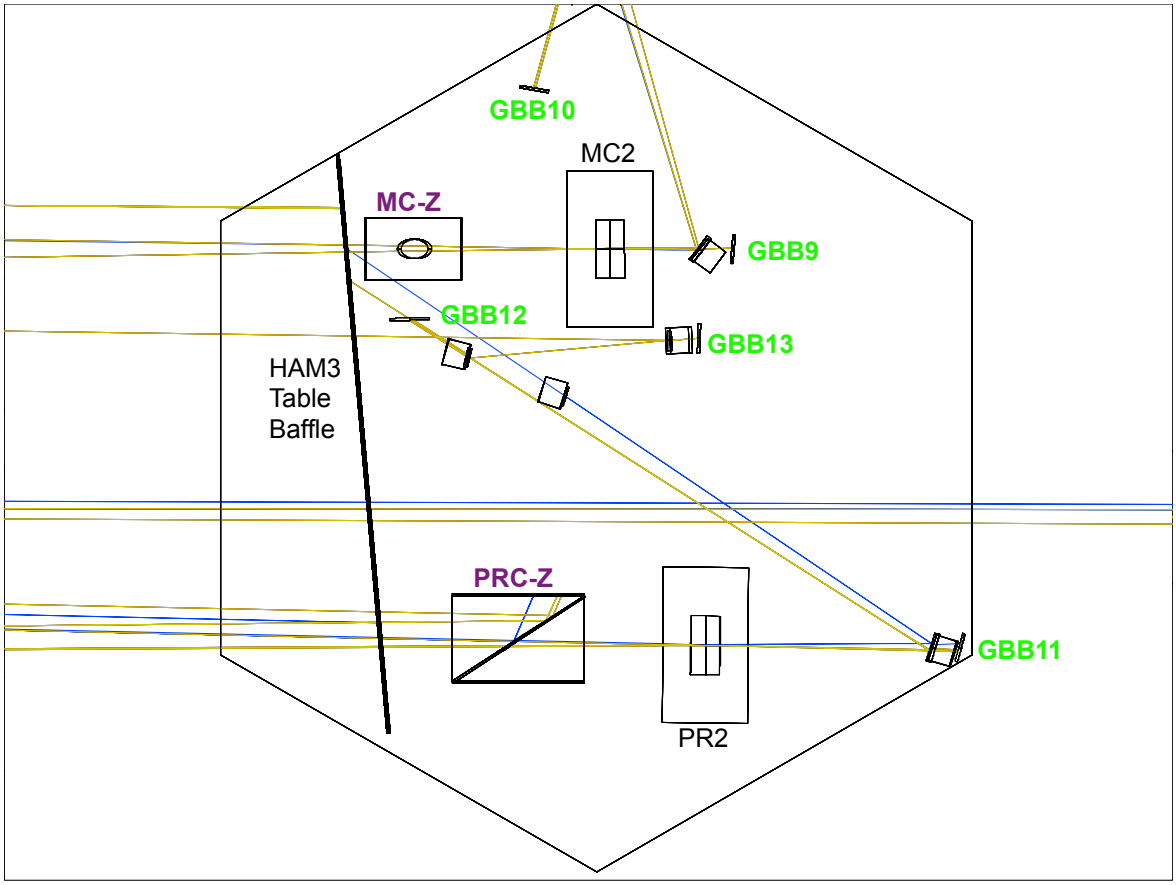

FIG. 14: Ghost beam baffles in HAM3

1. Beam blocks for the AR specular reflections from the HAM2 small transmissive optics

The majority of the ghost beams in HAM2 are caused by the AR coatings of the IO transmissive optics: the 7 crystals of the Faraday isolator and the HWP1 and AOE1, upstream from these and AOE2 downstream, toward SM2. By orienting these optics ~ 5 *mrad* w.r.t. the beam axis, we can redirect these beams from propagating into the IFO and dump them on low scattering surfaces.

Although they do not carry high powers, if entering the interferometer, reaching the ISS photodiodes, or propagating to the REFL port, ghost beams can become a large source of phase noise for the interferometer.

The parameters of the beams incident on the FI optics are listed in Table XX below:

TABLE XX: Parameters of beams incident on crystals of FI

Incident Forward Power	150 W
Incident Backward Power	$< 15\ W$, when in Science mode
Beam size	2.1 mm - 2.2 mm

The ghost beams were analyzed in ZEMAX for the parameters listed in Table XXI below. The AR reflection coefficients were either measured or reported in the vendor certifications and/or quotes.

TABLE XXI: Parameters for crystals of FI and small transmissive optics

Parameter	Units	2 x CWP (calcite wedge polarizer)	2 x HWP 1 x QR (quartz rotator)	2 x TGG (magneto optical element)	1 x DKDP (negative dn/dT material)	2 x AOE (adaptive optical element)
Material		Calcite	Quartz	Terbium Galium Garnet	Deuterated Potasium Di-hydrogen Phosphate	SF57
Index of Refraction		n_s=1.64237 n_p=1.47968	1.534	1.94366	1.4931	1.81174
Angle of Incidence	deg	6.5	0.286	0.286	0.286	0.286 (or less)
AR Coating Reflectivity	ppm	300	300	300	1000	300
Reflected Power / Surface						
from fwd beam	mW	45	45	45	150	45
from bkwd beam	mW	4.5	4.5	4.5	15	4.5
Bulk Absorption	% per cm	<1	-	0.15	0.5	0.04

The baffles blocking these ghost beams are listed in Table XXII.

TABLE XXII: Baffles blocking ghost beams from crystals of FI and small transmissive optics

AR ghost Beams	Baffle
HWP1 and AOE1	GBB5 on MC3 - AR side, with the FI isolation beam
CWP1	Blocked by HA4 and BW2
CWP2	Blocked by HA5, side of V1, and BW3
FI crystals	(for 5 mrad tilt of the crystals)
- from fwd beam	Back of HA2-b
- from bkwd beam	Back of HA12-a
AOE2	
- from fwd beam	in the REFL beam dump, for small AOI
	on the FI hard apertures, for AOI > 2 mrad
- from bkwd beam	3% inside the PR-Z scraper baffle (for 1-3 mrad tilt of AOE2),
	or on the HAM3 Table Baffle (for 4-5 mrad)
	97% at REFL, on the FI hard apertures, V1 (for ∼2 deg), or HA12-b

2. Beam blocks for the transmission through high reflectors and other low power beams

The baffles and their parameters are listed in Table XXIII.

TABLE XXIII: Other Ghost Beam Baffles Parameters

Bafle	ZEMAX Name	Beam Size (mm)	AOI (deg)	Max. Incident Power (W)	Material	DCC#
AR Dump (from SP-VP Window)	GBB1	2.2	5	4.50E-02	PSS	D1003018
S1 HR-trans	GBB2	2.12	5	1.85E-03	PSS	D1003010
S2 HR-trans	GBB3	2.12	7	1.85E-03	PSS	D1003010
MC1-AR specular	GBB4	2.1	5	5.55E-02	PSS	D1003010
MC3-AR Faraday Isolation	GBB5	2.1	5	1.50E+00	SiC	D1003044
SM1-HR trans return	GBB6	2.12	56	7.50E-04	PSS	D1003049
PMMT1 HR-trans	GBB7	2.16	7	7.50E-03	PSS	D1003045
PMMT2 HR-trans	GBB8	1.89	7	7.50E-03	PSS	D1003045
MC2 HR-trans, M-HR trans	GBB9	3.4	5	1.40E-05	PSS	D1003010
MC2 HR-trans VP-AR specular	GBB10	4	5	8.40E-05	PSS	D1003010
PR2 HR-trans M1-trans	GBB11	6	15	1.25E-04	PSS	D1003010
PR2 HR-trans M2-trans	GBB12	5.5	54	6.25E-05	PSS	D1003010
PR2 HR-trans M3-trans	GBB13	5.3	5	6.25E-05	PSS	D1003010

F. Baffle for Specular Reflections from PRM-AR Side

A ZEMAX representation of the ghost beams from the AR side of PRM is shown in Appendix B, Figure 35.

Table XXIV shows the powers in the PRM ghost beams for 150 W incident on PRM from IO, and 10% rejected from PRC for the first HR bounce when IFO is locked, while subsequent bounces transmit 3%.

TABLE XXIV: Power in the PRM ghost beams

Beam	Power
PRM-GBAR1	15 mW
PRM-GBAR2	1.46 mW
PRM-GBAR3	0.14 μW
PRM-GBHR1	45 μW
PRM-GBHR2	4.4 nW

TOWARD IO:

No new baffles need to be designed to collect the ghost beams from the AR side of PRM. The direct AR reflected beam is dumped on HA12-b, the side toward SM2, while the second and third order reflections (after one and two reflections on the HR side) are collected on the SM2 suspension baffles BW4 and BW5. For the specified AR reflectivity of 100 ppm (with a goal of 50 ppm), only the first two order reflections on the AR side of PRM are notable. The AR beams toward Input Optics are shown in Figure 15.

TOWARD IFO:

Toward the IFO, the ghost beams from PRM-AR side are blocked by the HAM2 table baffle or a separate PSS plate at the edge of the HAM2 table. Scaled by the finesse of the PRC, only the first order reflection on the HR side has comparable magnitude.

G. Baffle for Specular Reflections from PR2-AR Side

The ghost beams from the AR side of PR2 are shown in Appendix C, Figure 36.

The power in the PR2 ghost beams is listed in Table XXV below. We assumed 2.5 kW one-way incident power on PR2 when IFO is locked. Two beams correspond to each of the power values in the table, one from the beam coming from PRM, another from IFO.

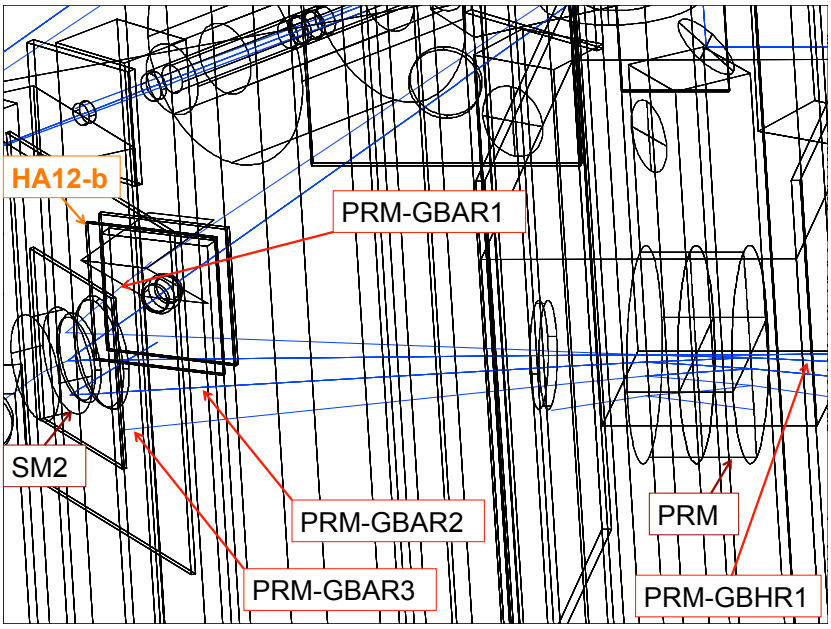

FIG. 15: Ghost beams from PRM-AR side toward IO are reflected off SM2 and blocked by HA12-b.

TABLE XXV: Power in the PR2 ghost beams

Beam	Power
PR2-GBAR1	0.2 mW
PR2-GBAR2	56 nW
PR2-GBHR1	47 nW

Only PR2-BGAR1 carries a power that is worth tracking, but Figure 16 shows few more AR ghost beams on the HR side also. The PR2-AR ghost beams toward PRM are collected by the PRC scraper baffle PRC-Z and a separate PSS plate at the edge of the HAM2 table. The ghost beams transmitted through PR2 are blocked by the HAM3 table baffle.

Scattering from these beams is studied in Section V.

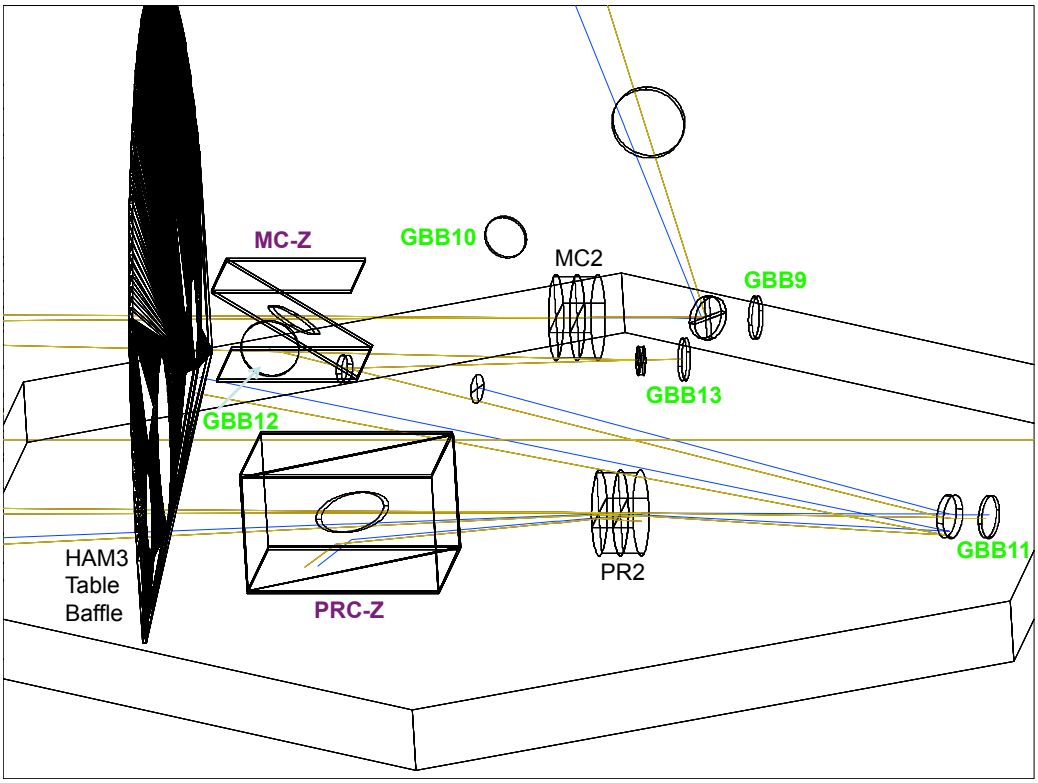

FIG. 16: Ghost Beams from PR2-AR toward PRM are collected by PRC-Z, and the first order transmitted through PR2 are blocked by the HAM3 table baffle.

V. SCATTERING IN THE IO SECTION

A. Scattering Considerations and Sources of Scattering

Scattering is a major source of phase noise for the interferometer, when it originates from surfaces that move horizontally in the low frequency band and couples on different paths into the interferometer with random and fluctuating phase.

The magnitude of the phase noise created by scattering depends on the magnitude of the scattered field and of the displacement of the scatterer, and the point of entrance in the interferometer.

In Input Optics, the large number of optical components produces a considerable amount of scattered light, however it's not a major issue, since the amplitude and the frequency noise of the electric field is sensed and controlled before it enters the interferometer.

Scattering in Input Optics can be produced by the main beam scattering off the optical com-

ponents in its path *(self scatter)*, and by stray light that hits baffles, beam dumps or the walls of the chambers *(parasitic scatter)*.

1. Self Scatter

Self scatter light is produced mainly by the 7 crystals of the Faraday isolator and SM2 for which the scattered light can propagate in the IFO without being sensed in the ISS loop.

2. Parasitic Scatter

Parasitic scatter is produced by ghost beams from reflection on the AR coatings of the crystals of the FI, AOE, PRM in HAM2, and PR2, ITM, CP and BS in HAM3, scattering off hard apertures, scraper baffles and ghost beam baffles. Also, it includes scattering from main beams stored on beam dumps, as well as light reaching the walls of the vacuum chambers.

B. Requirements for Scattered Light in Input Optics

The requirements for scattering in the IO section are derived in LIGO-T0900501 [7].

C. Scattering Calculations

Scattering calculations from all sources listed above are explicitly shown in T1000011-v2 [8].

The amount of power P_{sc} scattered into the interferometer directly from a scattering source (self-scatter) is determined by:

$$P_{sc} = P_{inc} \cdot BRDF(2 * AOI) \cdot \Delta\Omega \tag{1}$$

Where P_{inc} is the power incident on the scattering source, BRDF is the Bidirectional Reflectance Distribution Function of the surface of the scatterer estimated at twice the angle of incidence, $\Delta\Omega$ is the solid angle of the beam at the scattering source, which determines the coupling of the scattered light to the main beam and to the IFO. The BRDF function is the fraction of light scattered per unit solid angle, and for optics it is determined by the substrate microroughness, coating defects and contamination level.

The same relation 1 holds when scattering is produced by the main beam scattering directly into the REFL beam and is sensed in the Common Arm Loop, which senses the frequency noise between the laser and the interferometer. For scattering sensed directly by the intensity stabilization photodiodes, $\Delta\Omega$ represents the acceptance angle of the ISS-PD.

For parasitic scattering from ghost beams produced by AR coatings of transmissive optics, the amount of scattered light is given by:

$$P_{sc} = P_{AR}^{baffle} \cdot BRDF^{baffle}(AOSc) \cdot (\frac{A_{beam\ at\ optic}}{d^2_{baffle-optic}}) \cdot BRDF^{optic}(AOSc) \cdot \Delta\Omega_{towardSensingPort} \quad (2)$$

This relation is an example of scattering produced by an AR ghost beam collected by a baffle with $BRDF^{baffle}$ and then scattered to the sensing port via a suspended optic with $BRDF^{optic}$ in the solid angle of the beam. The two BRDF functions are estimated at the scattering angle $AOSc$, measured from the specular reflection for each surface. $A_{beam\ at\ optic}$ is the area of the main beam at the location of the directing optic, and $d_{baffle-optic}$ is the distance between the baffle (first scattering source) and the optic (second scattering source).

This is the case for scattering from the AR reflections from the crystals of the Faraday isolator, that are dumped on HA2-b and HA12-a hard apertures. The light scattered off these baffles then couples to the IFO or the REFL port via PMMT1 or PMMT2, in addition to back scatter via the AR surfaces of the crystals.

1. Parameters Used

a. BRDF Functions

The BRDF functions used in scattering calculations are listed in T1000011-v2 [8]. For convenience, we are including representative low scattering angle BRDF functions measured for super-polished ILIGO COC ([9], [13]).

$$BRDF_{(CSIRO\ S/N2)}(\theta) = \frac{2755}{(1 + 8.508 \cdot 10^8 \cdot \theta^2)^{1.24}}\ (sr^{-1}) \quad (3)$$

$$BRDF_{(GO\ S/N5)}(\theta) = \frac{1000}{(1 + 5.302 \cdot 10^8 \cdot \theta^2)^{1.55}}\ (sr^{-1}) \quad (4)$$

A graphical representation of these functions is shown in Figure 17. We should mention that we used the conservative function CSIRO-SN2 to estimate scattering from suspended optics, and that

the Advanced LIGO optics have better surface quality. The calculations are thus overestimating the amount of scattering by a factor of 10-100. This will assure us that we have sufficient safety margin when meeting the requirements.

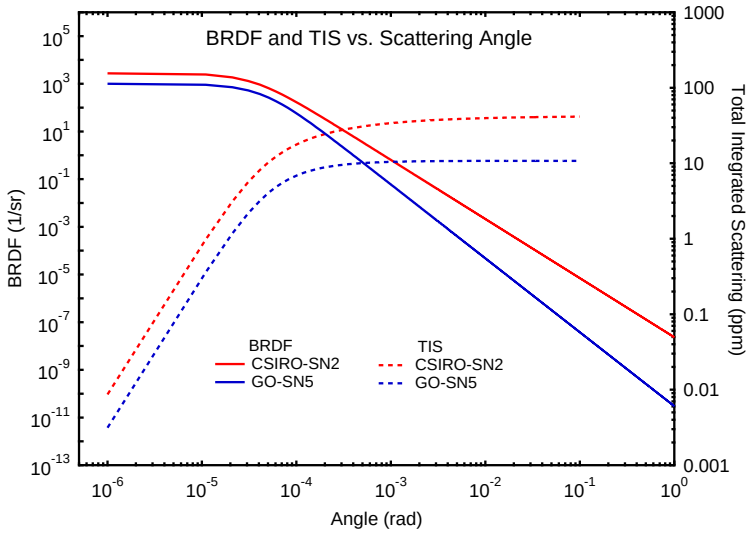

FIG. 17: BRDF functions determined from measured power spectral density data for iLIGO COC

b. Divergence Angles

Scattering calculations were carried out for the beam divergence angles shown in Table XXVI ([3], [4]).

TABLE XXVI: Beam divergence at different locations on the HAM2 and HAM3 tables

Beam	Beam waist, w_0 (mm)	Divergence (rad)	Solid angle (sr)
IFO, aLIGO	12	2.82E-05	2.50E-09
IMC	2.124	1.59E-04	7.99E-08
after PMMT1	0.9575	3.54E-04	3.93E-07
after PMMT2	1.019	3.32E-04	3.47E-07
after PRM	1.3	2.61E-04	2.13E-07
after PR2	0.113	3.00E-03	2.83E-05*

* approximate value

2. Summary of Results

The results of the scattering calculations are summarized in Tables XXVII - XXIX below (detailes in T1000011-v2 [8]).

TABLE XXVII: Scattering Results - Self Scatter

Source	P_{sc} (W)	$(P_{sc}/P_{in})^*_{calc}$	$(P_{sc}/P_{in})_{req}$
Backward reflected beam scattered into forward beam	3.99E-10	2.66E-12	< 4E-6
Forward beam scattered into REFL beam	3.99E-9	2.66E-11	< 3E-8
Scattering due to SM2 into the forward beam	1.56E-11	1.04E-13	< 1.6E-11

* The input power P_{in} was taken 150 W

TABLE XXVIII: Scattering Results - Parasitic Scatter

Source	P_{sc} (W)	$(P_{sc}/P_{in})^*_{calc}$	$(P_{sc}/P_{in})_{req}$
Scatt. from HA2-b into forward beam (via PMMT1)	7.74E-15	5.16E-17	< 4E-6
Scatt. from HA2-b into REFL beam (via PMMT1)	7.74E-19	5.16E-21	< 3E-8
Scatt. from HA2-b directly into ISS-PDs	5.43E-8	3.62E-10	< 1.6E-11
(placed a PSS baffle between HA2-b and the ISS-PD box)			
Scatt. from HA12-a into forward beam (via PMMT2)	5.24E-20	3.50E-22	< 4E-6
Scatt. from HA12-a into REFL beam (via PMMT2)	5.92E-16	3.95E-18	< 3E-8
Scatt. from HA12-b into forward beam (via SM2)	1.44E-18	9.63E-21	< 1.6E-11
Scatt. from HA12-b into REFL beam (via SM2)	1.64E-18	1.09E-20	< 3E-8
Scatt. from BW2 into ISS-PDs (via HA11)	<4.32E-11	<2.88E-13	< 1.6E-11
Scatt. from BW4 into the forward beam (via PRM)	2.43E-24	1.62E-26	< 1.6E-11
Scatt. from V3 into ISS-PDs	1.53E-10	1.02E-12	< 1.6E-11
Scatt. from V2 into forward beam (via PMMT2)**	1.19E-22	7.95E-25	< 4E-6
Scatt. from V2 into REFL beam (via PMMT2)**	1.35E-13	8.98E-16	< 3E-8
Scatt. from PR2-GBAR1 into IMC (via MC2)**	8.53E-22	5.69E-24	<4E-6, <1E-10
Scatt. from PRC-Z (ITM, CP, BS) into PRC (via PRM)	3.02E-16	2.01E-18	<1E-9
Scatt. from PRC-Z (ITM, CP, BS) into PRC (via PR3)	9.59E-18	6.40E-20	<1E-9
Scatt. from PRC-Z (ITM, CP, BS) into PRC (via PR2)	1.22E-14	8.12E-17	<1E-9

* The input power P_{in} was taken 150 W

** These beams have the wrong polarization and should be selected out by the CWP or not couple to the MC cavity. In these calculations we assumed that these beams have the right polarization to couple to the above ports.

TABLE XXIX: Scattering Results - Parasitic Back-Scatter

Source	P_{sc} (W)	$(P_{sc}/P_{in})^*_{calc}$	$(P_{sc}/P_{in})_{req}$
Back-Scatter from HA2-b baffle into REFL beam (via FI AR)	2.32E-12	1.55E-14	< 3E-8
Back-Scatter from HA12-a baffle into IFO (via FI AR)	1.01E-12	6.72E-15	< 4E-6
Back-Scatter from HA12-b baffle into IFO (via PRM HR-AR-HR)	4.91E-15	3.28E-17	< 4E-6
Back-Scatter from HA12-b baffle into the REFL beam (via PRM AR)	5.21E-14	3.47E-16	< 3E-8
Back-Scatter from HAM2 Table Baffle into IFO (via PRM HR-AR-HR)	2.88E-18	1.92E-20	< 1E-9
Back-Scatter from HAM3 Table Baffle into IFO (via PR2 AR-HR)	3.20E-19	2.13E-21	< 1E-9
Back-Scatter from PRC-Z into IFO (via PR2 HR-AR-HR)	9.39E-27	6.26E-29	< 1E-9
Back-Scatter from REFL beam dump into IFO	1.08E-11	7.19E-14	< 4E-6
Scatter from REFL BD to chamber walls, then back-scatter into IFO	1.62E-12	1.08E-14	< 4E-6
Back-Scatter from FI loss beam dump (V2) into REFL beam (via CWP2)	5.21E-12	3.47E-14	< 3E-8
Back-Scatter from ghost beam baffles behind high reflectors (e.g. PMMT)	7.37E-15	4.91E-17	< 3E-8
Back-Scatter from ITM, CP, BS AR beams from PRC-Z (BS entry port)	2.44E-10	1.63E-12	< 1E-9

D. Scattered Light Displacement Noise

The requirement for the scattered light displacement noise is determined in the AOS Preliminary Design [10] as:

$$\sqrt{\sum_{i=1}^{n}\left(\frac{SNXXX}{DARM}\cdot\frac{4\ \pi\ x_s}{\lambda}\cdot\sqrt{\frac{P_{SNi}}{P_0}}\right)^2} < \frac{1}{10}\cdot L\cdot h_{min} \tag{5}$$

where $SNXXX/DARM$ are the scattered light noise transfer functions for various injection points into IFO, determined by Hiro in [11] and shown in Fig. 18 a) for the ports relevant for IO. P_{SNi} is the scattered power into the IFO mode from various scattering sources, P_0 is the input laser power into the interferometer and x_s is the spectral density of the longitudinal motion of the scattering surface. L is the arm length of the interferometer and h_{min} is the minimum gravity wave spectral density requirement determined by the suspension and test mass thermal noise.

Light scattered in the IO section can be injected in the interferometer through PRM, or BS on the PRC side. The scattered light noise transfer functions for these injection points are shown in Fig. 18 a).

The most problematic sources of scatter in IO are placed on the HAM table, but a few ghost or scattered beams hit the chamber walls, or baffles that are connected to the chambers. For the HAM table we used the Advanced LIGO requirement, and for the chamber motion we used a sketch

fit to ground spectra measured by Jeff Kissel in [12]. The motion of these two sources is shown in Fig. 18 b).

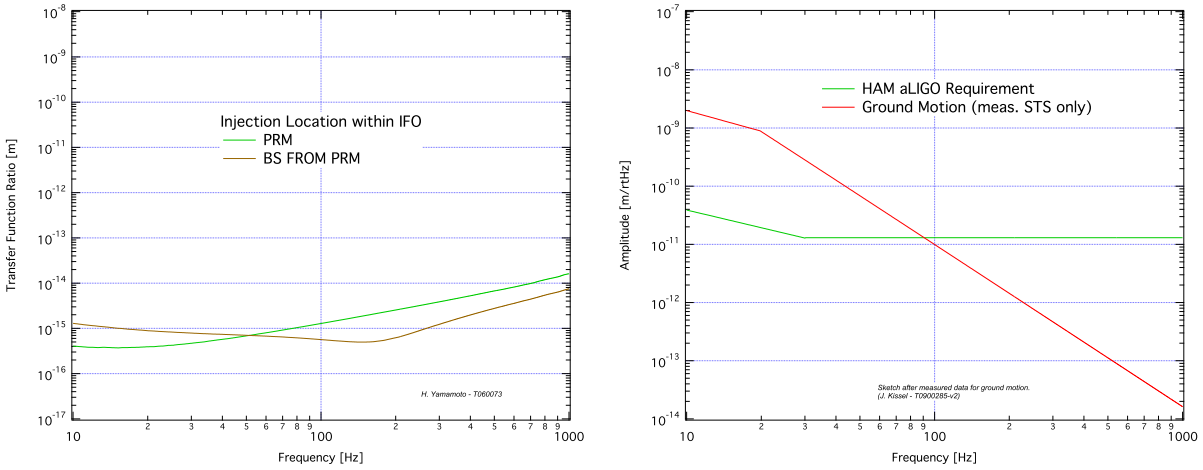

a) b)

FIG. 18: a) Scattered light noise transfer functions for PRM and BS FROM PR injection points into IFO relevant for Input Optics. b) The Advanced LIGO requirement for the motion of the HAM chamber and a sketch after measured ground motion [12]

A detailed list of scatter sources and powers coupled from the IO sections into the IFO mode is presented in T100011-v4. Table XXX shows a summary of these powers, the injection points into IFO and the motion of the scattering source.

TABLE XXX: Summary of scattered powers at different IO injection points into IFO

IO cumulative scattering sources	Injection	Motion	Power (W)
Components on HAM2 table	PRM	HAM	1.20E-08
HAM2 beams hitting chamber walls	PRM	Ground	4.85E-14
PRC-Z baffle	BS from PRC	HAM	2.44E-10
Large HAM2,3 table baffles	BS from PRC	Ground	3.20E-18

The dominant contribution to displacement noise in the IFO is from the optical components on the HAM2 table. In particular, this is direct scatter from the crystals of the Faraday isolator, which are placed close to normal incidence in the high optical power beam. The calculations are still conservative, since they do not include the reduction in the scattered power due to the AR coatings (a factor of 1000).

The Noise displacement calculated for all these sources is shown in Fig. 19.

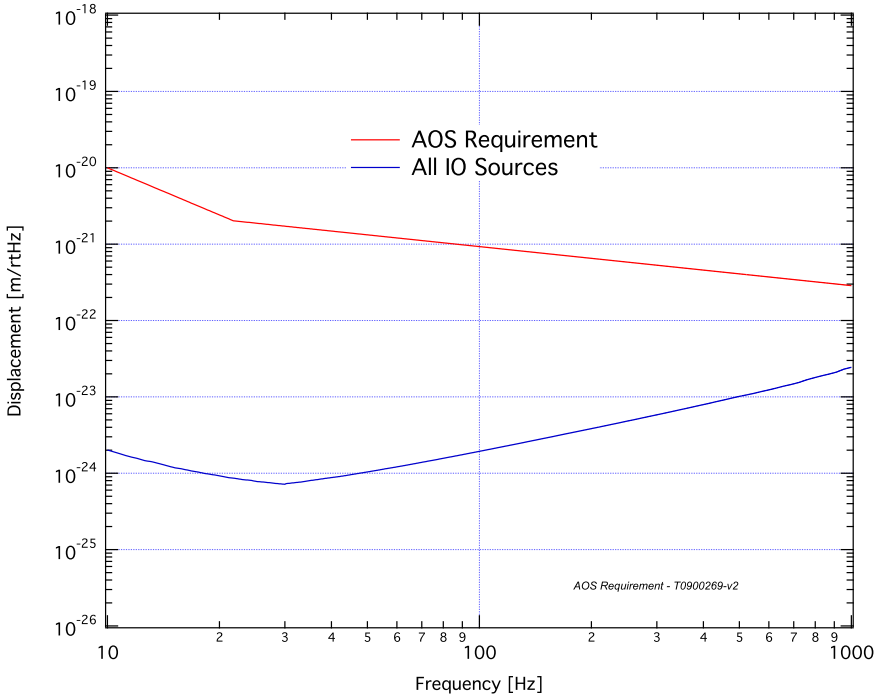

FIG. 19: Displacement noise in the IFO produced by scattered light in the IO section

The AOS requirement is well met over the 10-1000 Hz range.

VI. BAFFLE MATERIALS

A. Silicon Carbide

It has long been recognized that SiC is an excellent high temperature material for fabricating electronics, optics, and optoelectronics. Silicon carbide is often used as a layer for the very high temperature boilers to keep the temperature uniform due to its high thermal conductivity that surpasses that of Aluminum. Silicon carbide provides the mechanical stability due to low thermal expansion coefficient, high hardness, and rigidity. Apart from this, SiC is a low cost material that can be purchased quickly from various companies such as Saint Gobain, Coorstek, etc. There are various types of SiC available. The most pure form of it is called sintered SiC. This type is intended for high vacuum application. To test the feasibility of SiC as a baffle material, we bought a 6" x 6", 0.25" thick unpolished SiC and tested it under various conditions.

When CVD SiC coated, silicon carbide can be polished to sub-Angstrom micro-roughness, making it ideal for those baffles where scattering is a concern for the proper operation of the interferometer. We also purchased a few 1" CVD coated super-polished SiC samples to test reflectivity and scattering properties.

1. Reflectance Measurements

We measured the reflectivity of the 1" SiC superpolished sample as a function of angle of incidence. The measurements were performed for both p and s polarizations, at about 100 mW laser power and with a 1.4 mm beam diameter. The results are shown in Figure 20.

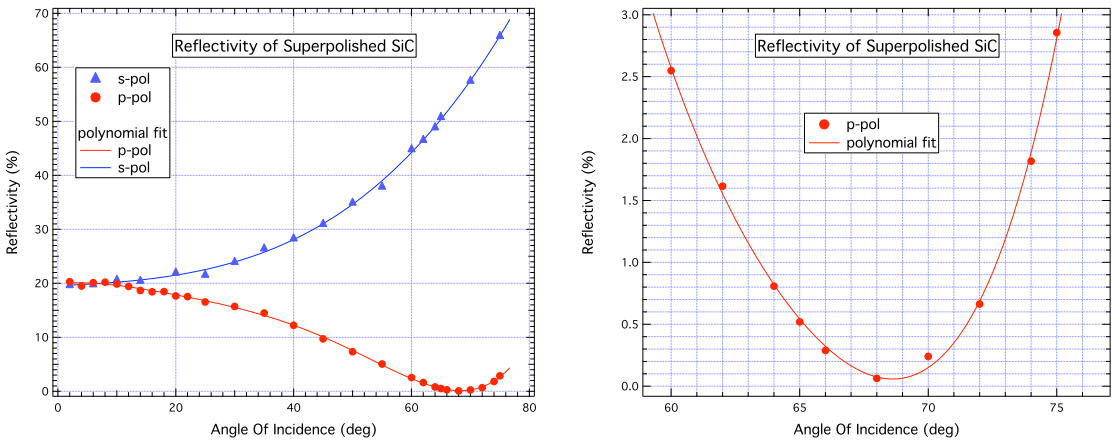

FIG. 20: Reflectivity of super-polished SiC vs AOI

At Brewster's angle, the reflectivity is less than 1000 ppm [19]. From the graph we determine the Brewster's angle as 68.5 deg, which agrees closely with what was derive from the refractive index reported in the literature [20].

2. Scattering Measurements

Scattering on superpolished SiC samples similar to what will be used in Advanced LIGO has been measured by Chris Francis and Josh Smith at the California State University Fullerton [14] and the results show that BRDF is comparable with black glass.

The results are summarized in Table XXXI below.

TABLE XXXI: Measured BRDF values for super-polished SiC

	Normal Incidence	Brewster's Angle
Black Glass	$BRDF \sim 5e^{-6}$ $(1/sr)$	$BRDF \sim 1e^{-5}$ $(1/sr)$
	$TIS \sim 13$ ppm	$TIS \sim 27$ ppm
SiC	$BRDF \sim 8e^{-6}$ $(1/sr)$	$BRDF \sim 6e^{-6}$ $(1/sr)$
	$TIS \sim 22$ ppm	$TIS \sim 15$ ppm

3. High Power Measurements

High Temperature Test in vacuum with 1.5 mm beam size

To further investigate the possibility of SiC use as a baffle material, SiC was exposed to a high laser power at the High Power Laser Facility (HPLF) at Livingston. SiC was placed inside a vacuum chamber with a high power laser beam focused at the SiC. The beam size was about 1.5 mm with about 80-90 W of laser power being incident on SiC. A number of thermocouples were attached to SiC to monitor the temperature. Particularly a thermocouple was attached to the back side of SiC as shown in Figure 21. The temperature of SiC as well as the pressure of the chamber was measured. The data is shown in Figure 22.

At the start of the test, the pressure in the chamber was 0.5 $\mu torr$ which increased to 15 $\mu torr$ in about 2 hours and then fell again to the initial 0.5 $\mu torr$. The RGA scan showed various combinations of Si and carbides (Fig. 23).

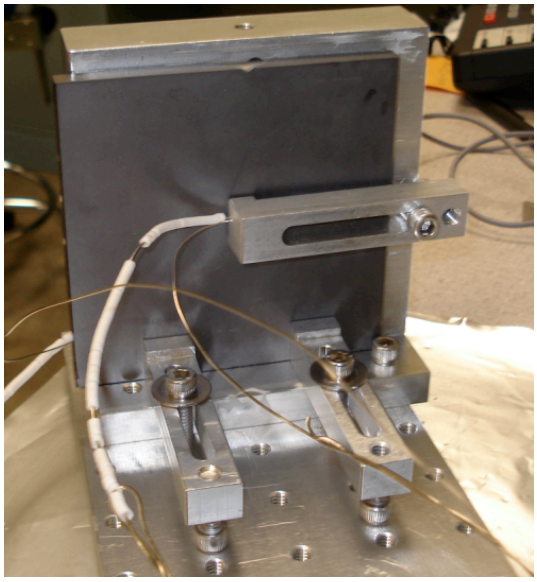

FIG. 21: Thermocouple attached to the back side of SiC directly behind the spot where the laser beam is hitting.

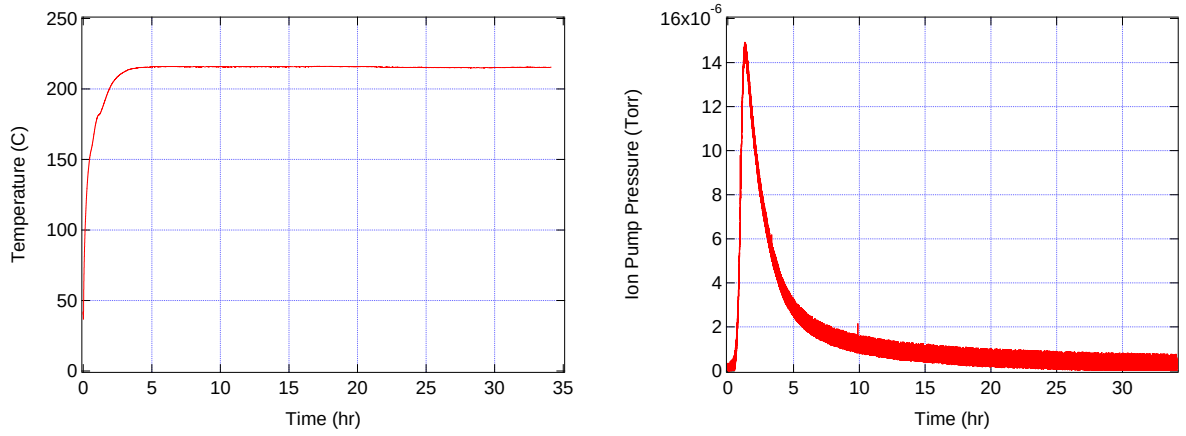

(a) (b)

FIG. 22: Temperature (a) and Pressure (b) of SiC measured at the rear surface under test at 80-90 W laser power beam focused to 1.5 mm spot size.

Also note that polished SiC has been tested elsewhere [15] at high temperature (about 1000 C) optically. The test showed no visible or optical damage. The test result showing reflected power from a SiC Fabry-Perot etalon of thickness 400 μm is shown in Figure 24.

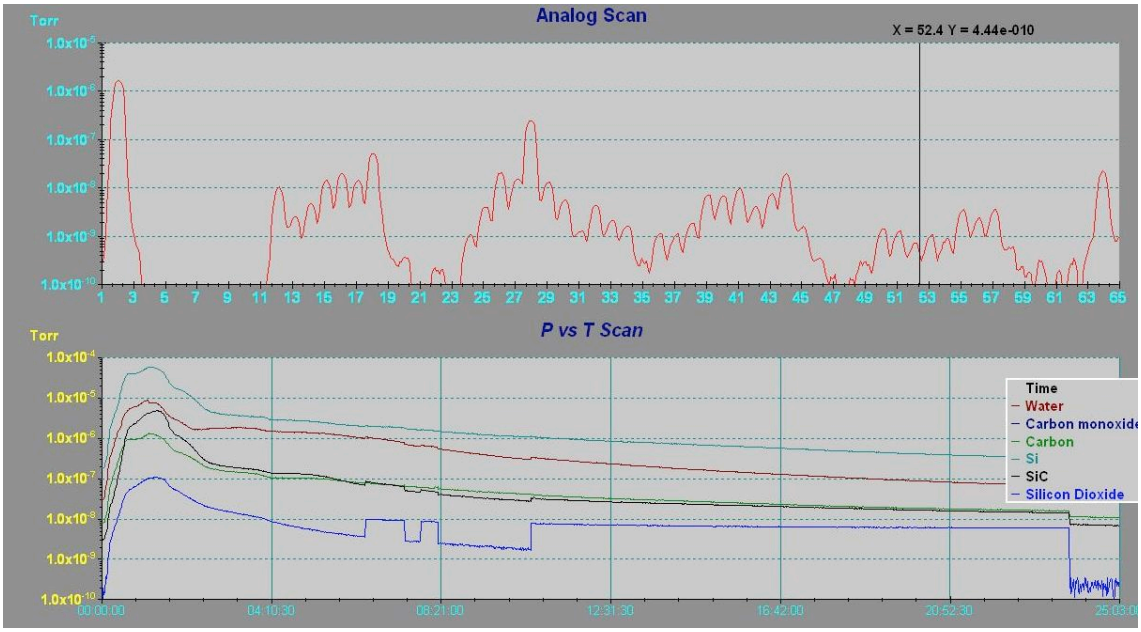

FIG. 23: RGA scan results for vacuum baked sintered SiC sample

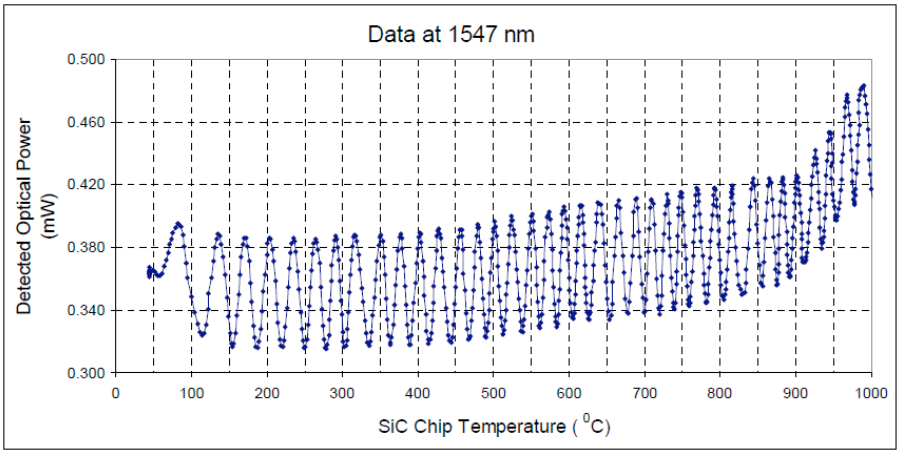

FIG. 24: SiC chip (400 micrometer thickness with both sides polished) reflectivity as a function of temperature.

High temperature test in vacuum with 200 μm **beam size**

In the first instant, a 200 μm beam with 80 W laser power was focused at SiC. This created a spark at the SiC surface. After inspection, some damage was observed as shown in Figure 25. However, as mentioned earlier, at 1.5 mm spot size no such damage is observed.

FIG. 25: Visible damage on SiC with 200 μm spot size and 80 W power.

4. Comsol Thermal Modeling

Two beam dumps will be required for the parking and REFL beams which will absorb powers approaching 180W over potentially long duty cycles. Due to the large amount of heat these baffles will need to dissipate, a Finite Element Analysis was performed in COMSOL with both designs in order to approximate the temperatures that result in both the Silicon Carbide (SIC) and Aluminum components of each baffle as well as the HAM2 table plate to which they are mounted. Our design goals were such that no baffle component should reach a temperature greater than its bake out temperature being 300C and 200C for Silicon Carbide and Aluminum respectively. An additional consideration is the final weight of each baffle which needs to be kept minimal due the constraints of the HAM2 mass budget.

Heat in these baffles is dissipated principally though contact with the HAM table. In our modeling the baffles were attached to a mock up of the HAM table whose boundary edge has a set temperature equal to the set ambient temperature of 27C. The models have been simplified by removing all fasteners and holes to enable a successful mesh of the solid. The laser spot size was defined for each baffle plate and appropriate inward heat flux set for that boundary according to a 180W laser beam. In the surface plot in Fig. 26 we see the parking beam dump with hot laser spot on the SIC plate. In our analysis we found that adjusting the cross sectional area of the aluminum side supports had a significant effect on the maximum temperature calculated at the laser spot. In our final design for the Parking beam dump we found a maximum temperature in the SIC plate of 236C. To find the peak temperature within the aluminum components we used a slice plot in order to view the hot area of aluminum directly behind the SIC plate as can be seen in Fig. 27.

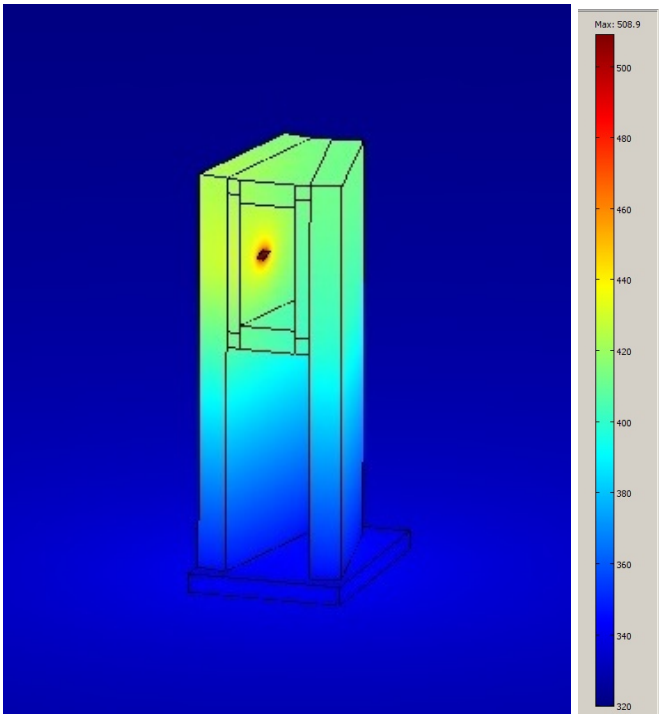

FIG. 26: Surface Temp Plot (Parking Beam Dump on HAM2 table)

The max temperature in our final design for the aluminum components given was 147C.

A similar analysis was performed on the REFL beam dump. The simplified model with the top half of the V-baffle removed is shown below. Again, with this baffle the cross section of the supporting aluminum components was adjusted to optimize both the weight and maximum temperatures found. The peak spot temperature found within the SIC plate for the REFL beam dump was 200C. A slice plot was again used to find the maximum temperature within the Aluminum mount which came to approximately 130C.

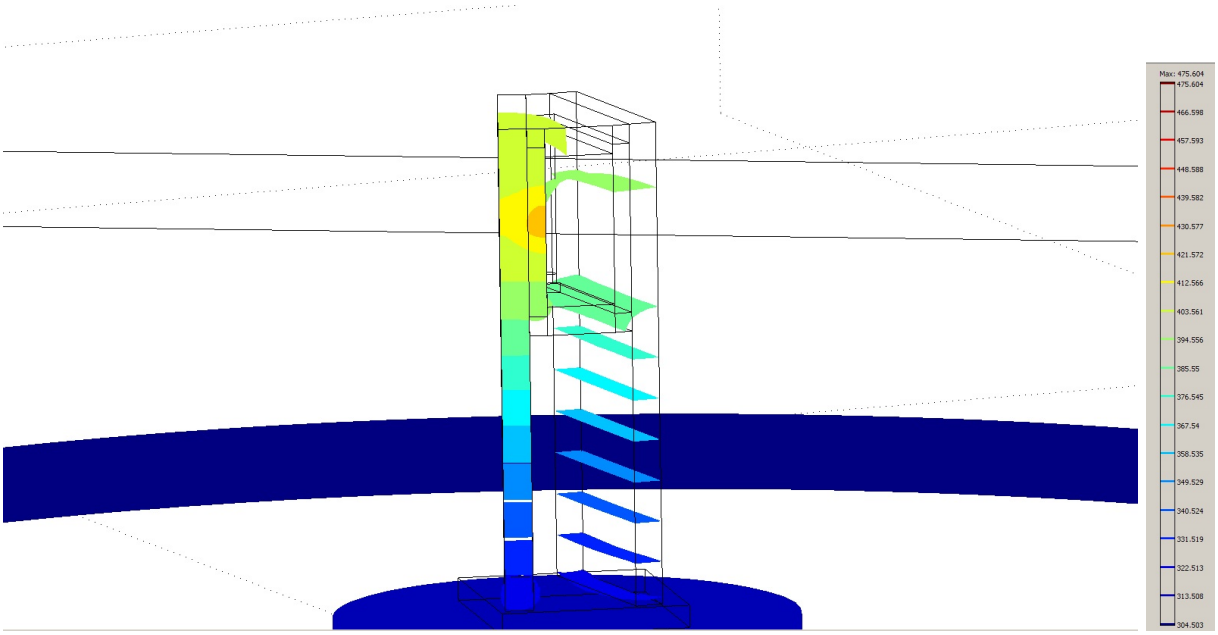

FIG. 27: Isotherm slice plot (Parking Beam Dump on HAM2 table)

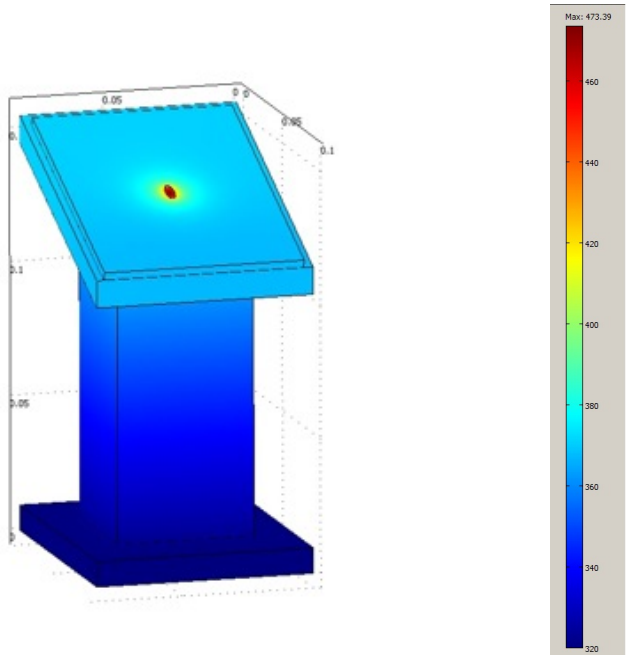

FIG. 28: Surface Temp Plot (REFL beam dump)

In the above steady state analysis the maximum temperatures within the HAM table plate were found to be above 20C in the vicinity of the baffle. It is possible that such a temperature increase within the HAM table will not be acceptable due to the effects it will have upon the

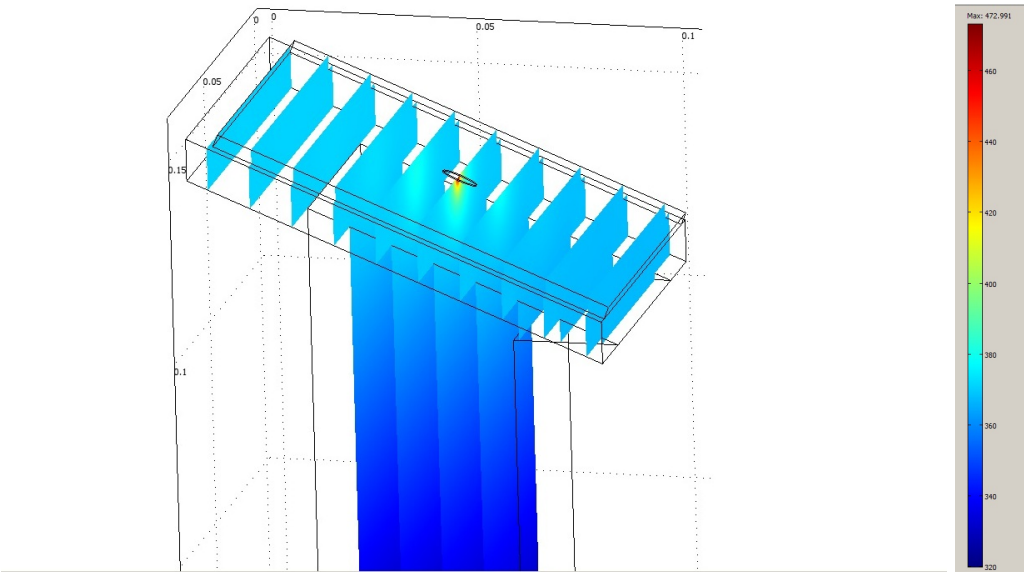

FIG. 29: Isotherm slice plot (REFL beam dump)

seismic isolation system below the table and as a result a transient analysis was performed in order to look at the time scale on which such a temperature rise will be seen.

For the purpose of the transient analysis we no longer set the HAM table edge to a fixed temperature but rather only allowed radiation heat loss. The plot in Fig. 30 shows the temperature

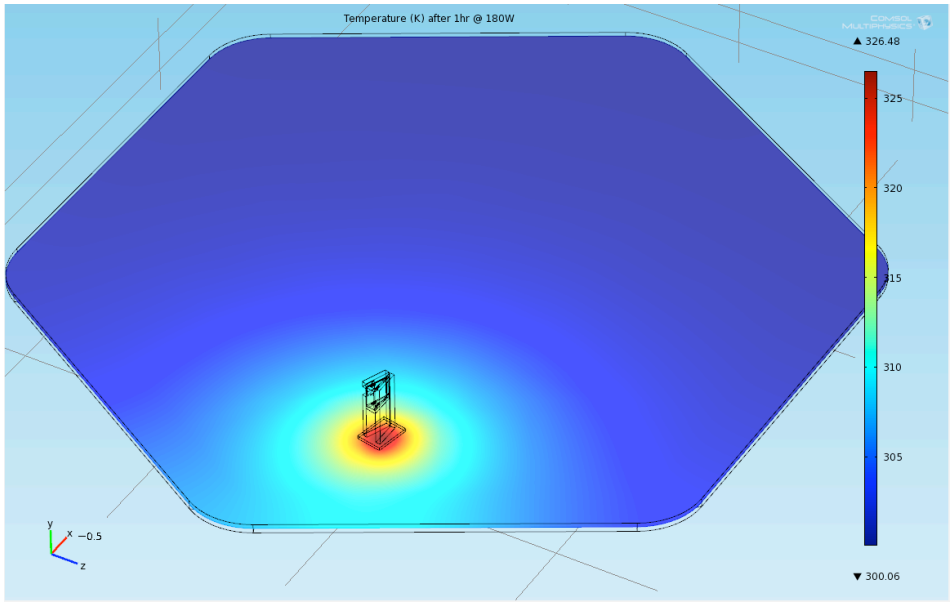

FIG. 30: HAM2 slice temperature after 1hr at 180W

of a slice midway through the HAM table after a time of 1hr with 180W incident power on the parking beam dump. Both ambient and initial temperatures were set to 300K. The maximum temperature rise found with the HAM table in this example is 26.5K.

Figure 31 is a graph of temperature vs time at fixed points 10, 20, 30 and 40 cm from the center of the beam dump within the HAM table. As it can be seen in the graph the temperature rise at a distance of 40cm from the baffle has fallen to 5K.

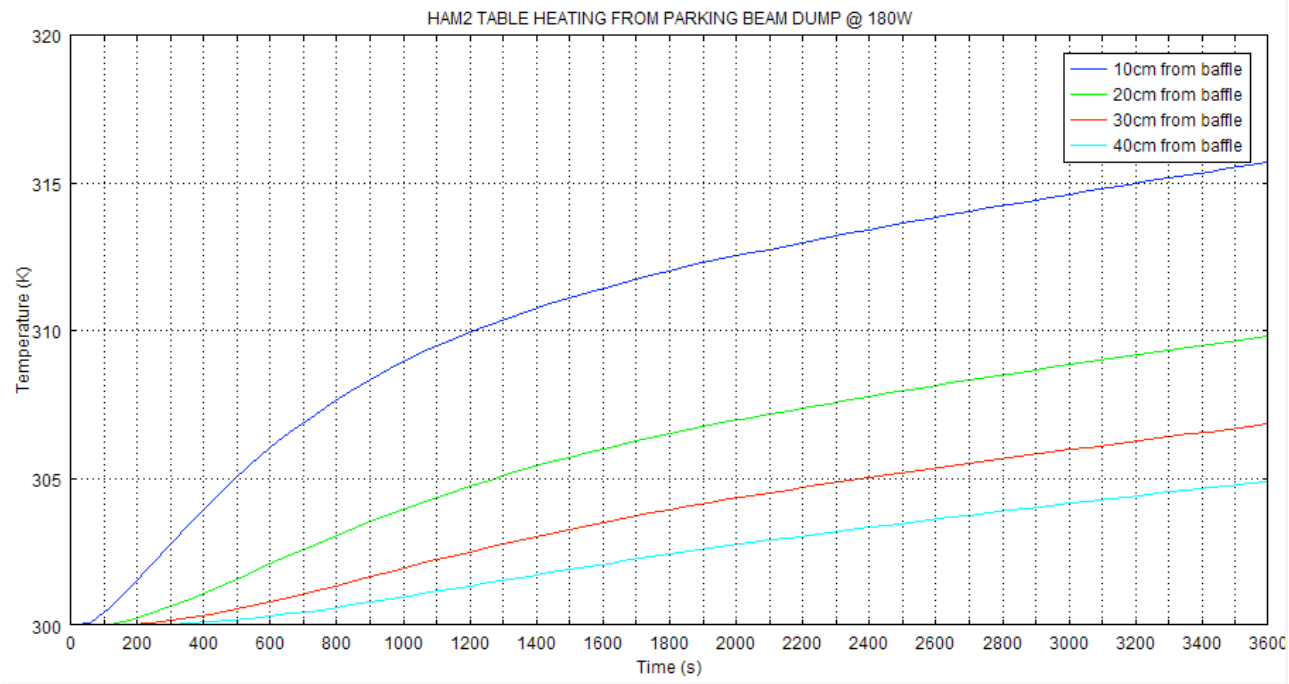

FIG. 31: HAM2 table temperature at various distances from parking beam dump over 1hr.

It may be the case that these temperatures will not be acceptable for proper seismic equipment operation and will warrant moving one or both parking beam dumps to a location other than the HAM table.

5. Vacuum Compatibility

An unpolished SiC sample was sent to Bob Taylor at Caltech for cleaning and baking. This sample successfully passed the baking test. It has not yet been tested in the cavity contamination experiment.

B. Porcelain Coated Steel

For those beams that carry moderately low powers, but which can either propagate randomly in the interferometer or on the alignment and sensing photodiodes, or scatter off rough surfaces and find paths to couple and disturb the proper operation of the different systems, we design low reflectivity, low scattering baffles made of porcelain (stainless) steel (PSS), which is well known and recognized for possessing these optical properties.

1. Reflectance Measurements

We measured the reflectivity of a 4" x 4" PSS sample borrowed from Mike Smith for the process used by AOS system. The results are shown in Figure 32.

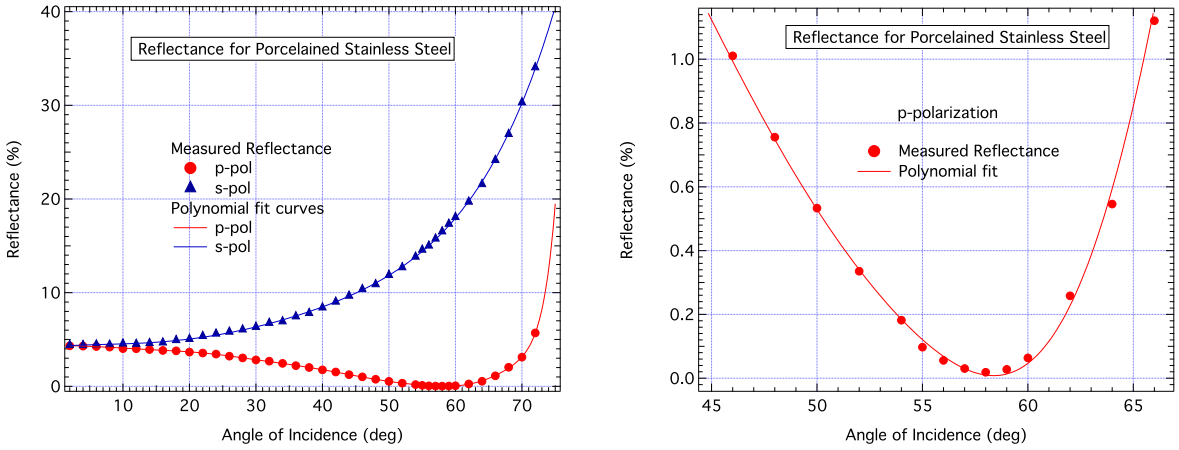

FIG. 32: Reflectivity of PSS vs AOI

This material will be used for all ghost beam baffles, the ISS scattering protective baffle and the two scraper baffles in the HAM3 chamber.

The scraper baffles will make use of the reflection at Brewster's angle of $\sim 58\ deg$, which is much smaller than for silicon carbide, hence will allow for smaller baffle footprint. In addition, the overall reflectance is significantly lower than for silicon carbide, and actually stays lower than 1000 ppm for a much wider range of angles of incidence (from 55 deg to 61 deg, compared to 60 deg to 70 deg for SiC).

2. Scattering Measurements

Scattering measurements on porcelainized steel were made a long time ago by Rai Weiss, indicating a back-scatter $BRDF < 0.05\ sr^{-1}$, independent of incidence angle for $\theta > 5\ deg$ [21].

3. Power Measurements

We also tested porcelain stainless steel sample at laser powers as high as 20 W, to determine the high threshold for its use in Advanced LIGO. The tests were done in air, close to normal incidence, for a beam about 5.5 mm in diameter. The power was increased in steps as shown in Table XXXII, and after each step we waited 2-5 minutes and checked for visual damage. No apparent damage

TABLE XXXII: PSS power test results

Power (W)	Intensity (W/cm^2)	Temperature (C)	Test results
1.3	6.1	97	OK
2.8	13.2	171	OK
6.0	28.3	270	OK
10.0	47.1	> 270	OK
13.4	63.1	> 270	OK
20.0	94.2	> 270	plate started glowing; crater $\sim$ 3mm diameter found after tests

has been observed until we increased the power to 20 W, when the plate started glowing, and then we reduced the power back to 13 W. Table XXXII summarizes the results and observations from the tests. For safety, we place the upper limit at 13 W/cm^2.

To check the temperature and the thermal distribution on the surface we recorded a few images with the thermal imaging camera, which are shown in Figure 33.

The temperature distribution across the baffle shows that the thermal conductivity of this material is fairly poor. The thermal imaging camera saturates at 270 C, so above 10 W the temperature could not be recorded, being higher than 270 C.

4. Manufacturing and Vacuum Compatibility

The manufacturing process is well understood and documented [16], [17], [18], and qualified vendors have been located by the AOS system. We plan to use the same vendors as AOS for the

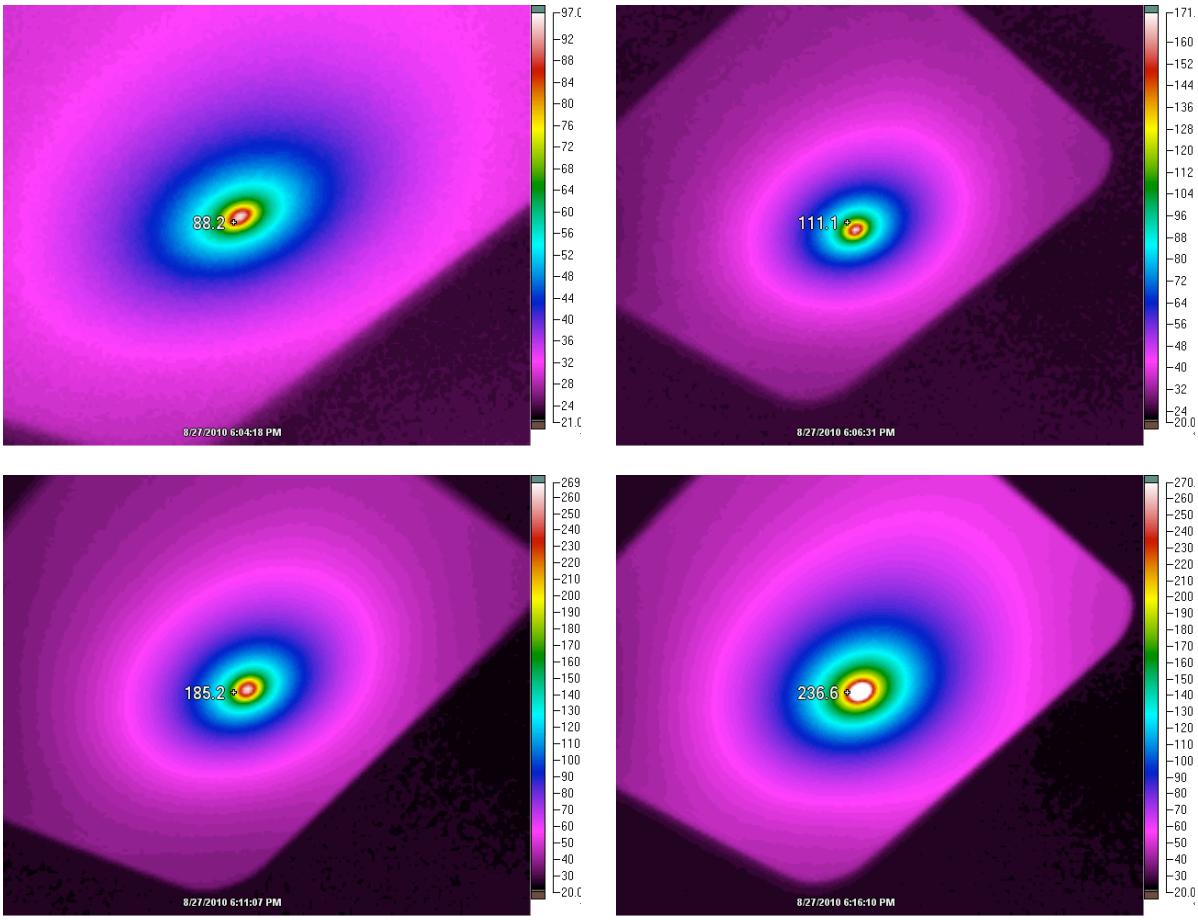

FIG. 33: Temperature distribution across the baffle recorded with a thermal imaging camera

procurement of the porcelain steel baffles.

Appendix A: FI losses estimate from isolation ratio considerations

A maximum deterioration in the isolation ratio from 50 dB to as low as 20 dB could be anticipated when Faraday Isolator is placed in vacuum and exposed to high optical power [22] This drop was modeled to correspond to a thermal depolarization or polarization mismatch in the TGG crystals of 5.6 deg, double passed (Fig. 34).

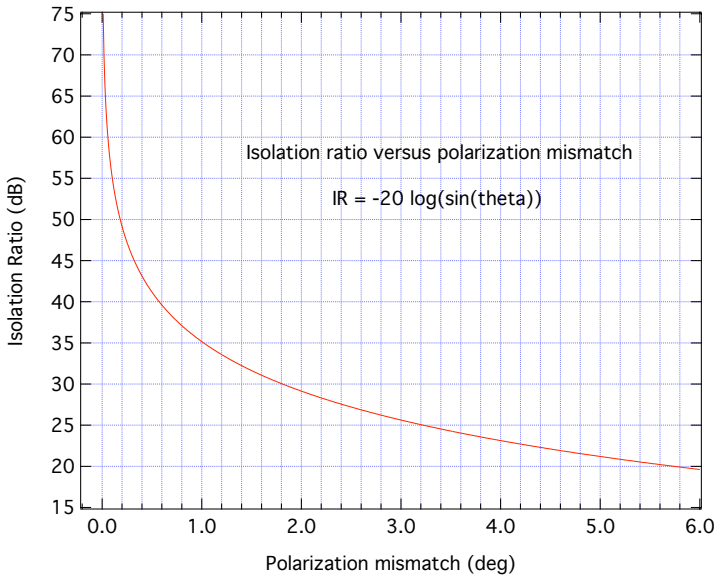

FIG. 34: Faraday isolation ratio vs polarization mismatch.

In the forward direction, the polarization mismatch will be 2.8 deg, determining the power in the wrong polarization as $sin^2(2.8\ deg) = 0.24\%$ of the input power. A 1% power loss is extremely conservative, corresponding to 5.6 deg polarization mismatch between the rotation in the TGG crystals and the second calcite wedge polarizer. The power in this beam would be most likely less than 400 mW.

Appendix B: PRM Ghost Beams

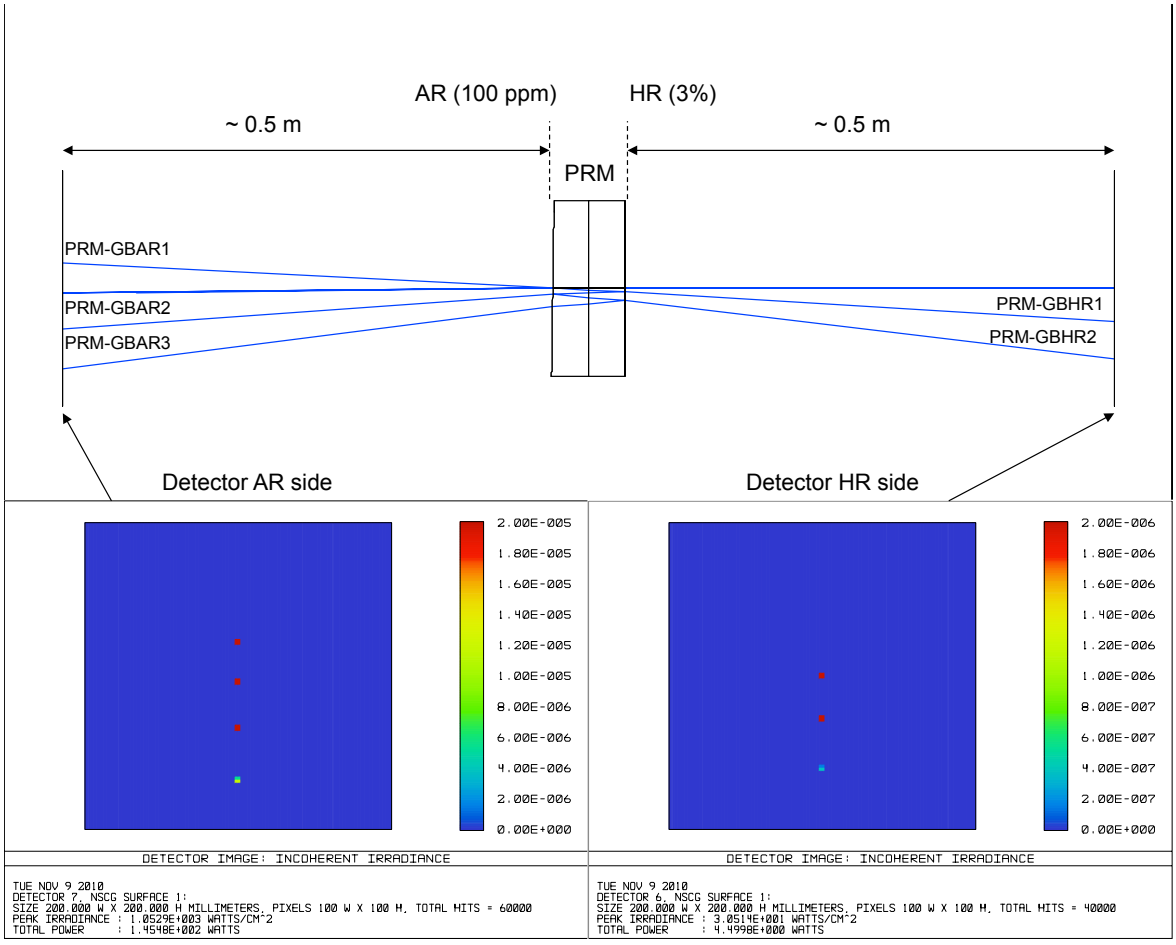

FIG. 35: PRM Ghost Beams (modeling assumes RC unlocked)

Appendix C: PR2 Ghost Beams

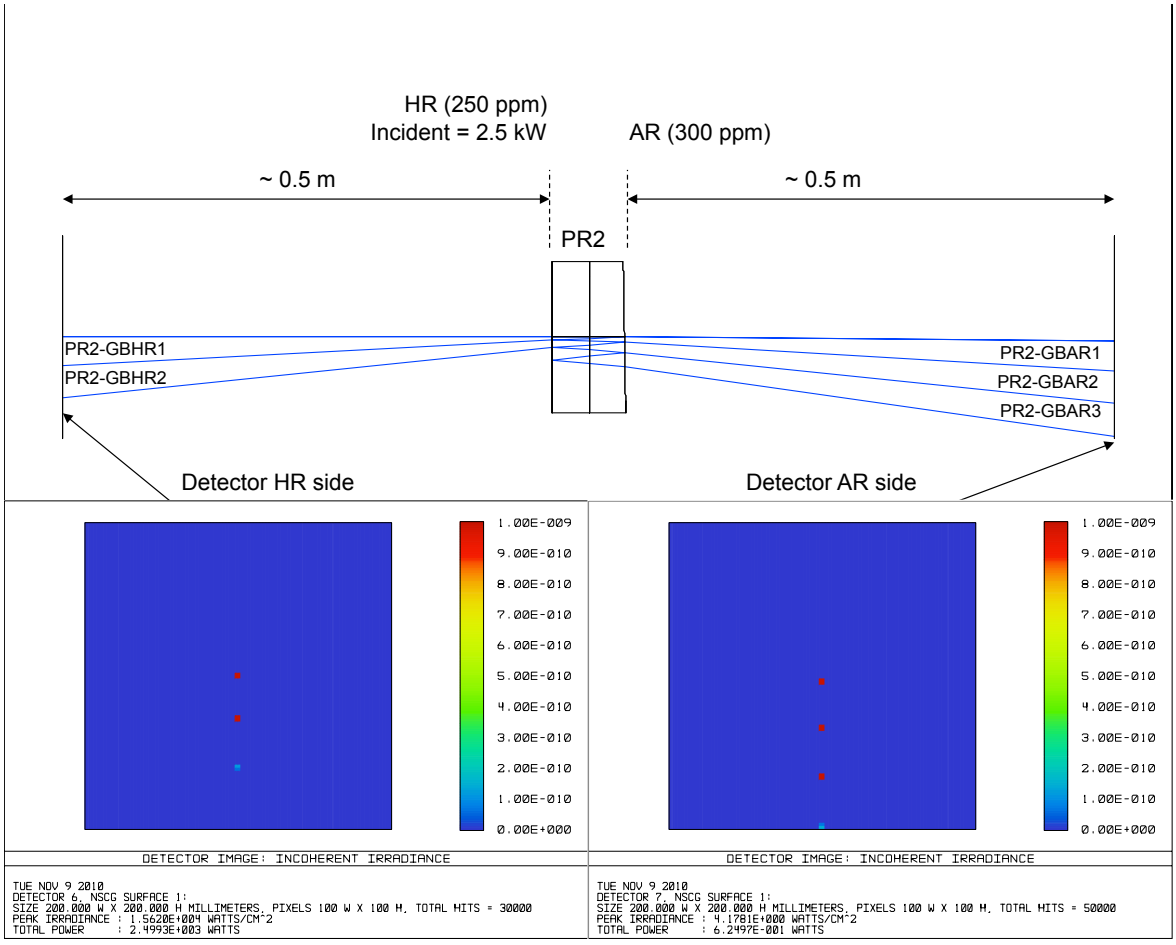

FIG. 36: PR2 Ghost Beams (modeling assumes RC locked)

[1] R. Martin, *"Advanced LIGO IO ZEMAX Baffle Layout - L1*, D1003114-v1

[2] L. Williams, *" ALIGO IO Layout LLO BCS*, D0900919-v2

[3] Muzammil A. Arain and Guido Mueller, *"Optical Layout and Parameters for the Advanced LIGO Cavities"*, LIGO-T0900043-10

[4] Muzammil A. Arain, et al, *"Pre Mode Matching Telescope Parameters, Adaptive Mode matching, and Diagnostics"*, LIGO-T0900407-v4

[5] Norna A Robertson, et al, *"HAM Small Triple Suspension Final Design Document"*, p.12 Table 1, T0900435-v3

[6] Giacomo Ciani, et al, *"HAM Auxiliary Suspensions Final Design"*, LIGO-T1000338-v3

[7] Guido Mueller, *"Requirements for Scattered Light in IO"*, T0900501-v2

[8] Rodica Martin, *"Calculations for Scattered Light in IO"*, T1000011-v4

[9] Michael Smith, *"Baffling Requirements for the 4K and 2K IFO"*, T980027-01-D

[10] Michael Smith, et al, *"AOS Stray Light Control (SLC) Preliminary Design"*, T0900269-v2

[11] Hiroaki Yamamoto, *"Transfer functions of scattered lights in AdvLIGO COC"*, T060073-00

[12] Jeff Kissel, *"L1 HAM6 ISI eLIGO Final Performance Measurements"*, T0900285-v2

[13] Albert Lazzarini, *"Inputs to Beam Tube Scattering and Optical Surface Roughness Requirement Analysis for Advanced LIGO"*, T060013-02-E

[14] Chris Francis, *"Measuring Scattered Light from Advanced LIGO Optics"*, Master Project, California State University Fullerton, G1000964-v1

[15] M. Arain, *Interferometry-based free space communication and information processing*, Ph.D. Dissertation, University of Central Florida, Orlando, FL, USA.

[16] A. Sibley, *"Porcelain Coating of Beam Tube Baffles"*, LIGO-E960028-A B

[17] Heidy Kelman, *"Process for Enameled Steel Sheet to be used in the LIGO Ultra-High Vacuum System"*, E1000083-v4

[18] Dennis Coyne, *"Material Qualification RGA Test Results: Ferro Corporation RM108 Frit"*, E1000221-v1

[19] These data do not have the background signal from the room lights subtracted, which was about 35 μW. When this is accounted for, we can infer about 300 ppm. We repeated the measurements in the HPLF with 85 W optical power, and determined 260 ppm reflectance at Brewster's angle. This clearly confirms very low reflectance at both high and low power levels.

[20] The refractive index reported at 1064 nm is about 2.575, determining a Brewster's angle of 68.78 deg

[21] Communication with Mike Smith, August 16, 2010

[22] The eLIGO Faraday isolator, which is a prototype for the Advanced LIGO isolator, was measured in situ in L1 for powers up to 18 W, and has shown a maximum deterioration ratio 25 dB, which did not degrade with the input power.